Laser-spectroscopy measurements of nuclear charge radii

Yu. P. Gangrskiĭ
Joint Institute for Nuclear Research, Dubna

Fiz. Elem. Chastits At. Yadra **23**, 1616–1664 (November–December 1992)

Experimental data on the differences of the charge radii in ground and isomer states are reviewed. The data were obtained by laser-spectroscopy methods. The relationship between the changes of the mean-square charge radii and the quadrupole deformation parameters is analyzed. The experimental data are compared with calculations made in various models (droplet model and others).

INTRODUCTION

The distribution of the electric charge in a nucleus is one of its most important characteristics. From it one can estimate the size and shape of the nucleus and obtain information about the interactions between its nucleons. Therefore, the investigation of this distribution is one of the traditional problems of nuclear physics, and a large amount of experimental data has by now been accumulated in this field.

One of the main methods of investigating the electric-charge distribution in the nucleus is the optical method. It is based on high-precision measurement of the energy levels of the electron shell of the atom, which are perturbed by the electric charge of the nucleus. The spatial distribution of the nuclear charge gives rise to shifts of the electron levels, while the magnetic moment of the nucleus splits them. Although these changes are very small (10^{-8}–10^{-6} of the energy level), they can be measured with high accuracy by modern methods of optical spectroscopy.

In recent years, tunable lasers have made it possible to develop these methods further. The unique properties of laser radiation—high monochromaticity (to 10^{-10} and better) and intensity (up to 10^{19} photon/sec on the average and by many orders of magnitude higher in a pulse), directionality, coherence—have made it possible to raise the accuracy and sensitivity of the measurements appreciably. This has made it possible, on the one hand, to measure small changes of the charge radii or nuclear moments in going from one isotope to another or from the ground to an isomer state, and, on the other hand, to investigate nuclei formed with low yields at the limit of nucleon stability or in unusual states. Laser radiation has been used in many experiments on the ground (or isomer) states of long chains (up to 20–25 nuclei) of isotopes of a single element. These investigations have greatly extended the information on a number of nuclear parameters—the charge radii, spins, magnetic dipole and electric quadrupole moments—and their dependence on the number of neutrons in the nucleus. A large proportion of this information was obtained for nuclei that could not be investigated by the old methods.

The aim of this review is to systematize the data on one of these parameters—the nuclear charge radius determined in measurements using laser radiation—to compare these data with various models (mainly the droplet model), and to discuss new data obtained by analyzing these results on nuclear structure and the role of collective and single-particle effects in different regions of nuclides.

DESCRIPTION OF THE ELECTRIC-CHARGE DISTRIBUTION IN NUCLEI

The first experiments in which charged particles were scattered by nuclei revealed a complicated distribution of the charge in them, both in the radial and in the azimuthal direction. The radial distribution is characterized by a constant density of charge over the volume with a small decrease in the center of the nucleus and a smooth decay at the boundary (Fig. 1). Various expressions based on models of the nucleus are used to describe this distribution. One of the most widely used expressions is the Fermi distribution: with two parameters[1]

$$\rho(r)=\frac{\rho_0}{1+\exp\dfrac{r-c}{a}} \tag{1}$$

or with three parameters

$$\rho(r)=\frac{\rho_0\left[1+\omega\left(\dfrac{r}{c}\right)^2\right]}{1+\exp\dfrac{r-c}{a}}, \tag{2}$$

where ρ_0 is the charge density at the center of the nucleus, determined from the normalization conditions:

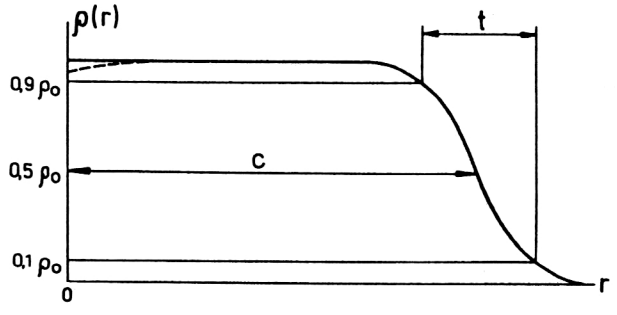

FIG. 1. Radial distribution of the electric charge in a nucleus (Fermi distribution); ρ is the charge density, and r is the radius of the nucleus.

 0090-4759/92/060704-22$04.00

$$\int \rho(r)dv=\rho_0\frac{4\pi}{3}c^3\left[1+\pi^2\left(\frac{a}{c}\right)^2\right]. \quad (3)$$

(From analysis of the experimental data, $\rho_0=0.17$ nucleon/fm^3.) Here, c is the half-density radius, ω is the parameter that describes the decrease of the density at the center of the nucleus, and a is the parameter of the surface layer, related to the distance over which the charge density decreases from $0.9\rho_0$ to $0.1\rho_0$ by the equation

$$t=(4\ln 3)a\approx 4.39a. \quad (4)$$

The values of these parameters are given below in the discussion of the experimental data and calculations based on the various models.

In a first approximation, it is assumed that the radial charge distribution does not depend on the azimuthal direction.

In many cases, especially in comparisons of experimental data for different nuclei in both ground and excited states, it is convenient to characterize the distribution of the electric charge by a single parameter—its mean radial moment of nth order:

$$\langle r^n\rangle=\frac{\int\rho(r)r^{n+2}dr}{\int\rho(r)r^2dr}. \quad (5)$$

For the Fermi distribution in the case of medium and heavy nuclei, when c is appreciably larger than a, this expression is usually represented as a series in powers of a/c:

$$\langle r^n\rangle=\frac{3}{n+3}c^n\left[1+\frac{n(n+5)}{6}\pi^2\left(\frac{a}{c}\right)^2\ldots\right]. \quad (6)$$

The moment that is most often used is the radial moment of second order—the mean-square charge radius:

$$\langle r^2\rangle=\frac{\int\rho(r)r^4dr}{\int\rho(r)r^2dr}. \quad (7)$$

The mean-square charge radius is related (up to second-order effects) to the parameters of the Fermi distribution by the equation

$$\langle r^2\rangle=\frac{3}{5}c^2+\frac{7}{5\pi^2}a^2. \quad (8)$$

For a nucleus with a sharp boundary and a uniform charge distribution (rectangular distribution)

$$\langle r^2\rangle=\frac{3}{5}R^2, \quad (9)$$

where R is the radius of the nucleus.

In some cases, the radial moments of higher orders, $\langle r^4\rangle$ and $\langle r^6\rangle$, are also considered. They are more sensitive to the electric multipole moments of higher orders (hexadecapole, etc.).

In many nuclei, the azimuthal distribution of the electric charge exhibits an appreciable deviation from spherical symmetry. This distribution is usually expressed as an expansion in spherical harmonics:[2]

$$V(\theta)=V_0(1+\beta_2Y_{20}(\theta)+\beta_3Y_{30}(\theta)+\beta_4Y_{40}(\theta)+\ldots), \quad (10)$$

where r_0 is the radius of a spherical nucleus of the same volume, $Y_{i0}(\theta)$ are spherical functions, and β_i are deformation parameters (quadrupole, octupole, hexadecapole, etc.). For such an azimuthal distribution, the mean-square charge radius has the form

$$\langle r^2\rangle=\langle r^2\rangle_0\left[1+\frac{5}{4\pi}(\beta_2^2+\beta_3^2+\beta_4^2)+\frac{5}{84}\left(\frac{5}{\pi}\right)^{3/2}\beta_2^3+\frac{1}{6}\left(\frac{5}{\pi}\right)^{3/2}\beta_2\beta_3^2+\frac{75}{28}\left(\frac{1}{\pi}\right)^{3/2}\beta_2^2\beta_4\right], \quad (11)$$

where $\langle r^2\rangle_0$ is its value for the spherical nucleus of the same volume. If none of the parameters β exceeds 0.3, then in the expression (11) a restriction may be made to the terms quadratic in β (the contribution from the remaining terms is less than 10%).

The deformation parameters are expressed in terms of the electric multipole moments of the same order:

$$Q_\lambda=\frac{3}{\sqrt{(2\lambda+1)\pi}}ZR^\lambda\beta_\lambda, \quad (12)$$

where λ is the multipolarity ($\lambda=2, 3, 4\ldots$), and $R=1.2A^{1/3}$ fm. For strongly deformed nuclei, for which it is necessary to take into account the parameters β of higher orders, the expressions for the quadrupole, Q_2, and hexadecapole, Q^4, moments are

$$Q_2=\frac{3}{\sqrt{5\pi}}ZR^2\beta_2\left(1+\frac{1}{8}\sqrt{5/\pi}\beta_2+\frac{5}{8\pi}\beta_2^2+\ldots\right), \quad (13)$$

$$Q_4=\frac{1}{\sqrt{\pi}}ZR^4\beta_4\left(1+\sqrt{\frac{3}{\pi}}\beta_2+\ldots\right). \quad (14)$$

Numerous methods of experimental determination of the electric multipole moments are known. One of the most popular methods is to measure the reduced probabilities of the electric transitions of the corresponding multipolarity λ. In the case of even–even nuclei and quadrupole moments, their values are determined by the reduced probabilities of transitions to a lower excited state with spin 2^+. In the remaining cases (odd nuclei and other multipole moments), it is necessary to take into account transitions to other excited levels as well:

$$B(E\lambda)=e^2\left|\sqrt{\frac{2\lambda+1}{16\pi}}Q_\lambda\right|^2, \quad (15)$$

$$\beta_\lambda^2=\frac{16\pi^2}{9Z^2R_0^{2\lambda}}B(E\lambda). \quad (16)$$

In spherical or weakly deformed nuclei, deviations from equilibrium shape arise as a result of surface vibrations:

$$\rho(r,\alpha_{\lambda\mu})=\rho_e(r)-R_0\frac{\delta\rho}{\delta r}\sum_{\lambda,\mu}\alpha_{\lambda\mu}Y_{\lambda\mu}, \quad (17)$$

where ρ_e is the charge density for the equilibrium shape, and $\alpha_{\lambda\mu}$, the coefficients of the deviation of order λ from the equilibrium shape, are related to the deformation parameters by the equation

$$\beta_\lambda^2=\sum_\lambda \alpha_{\lambda\mu}^2.$$

These parameters of the dynamic deformation, like those of the static deformation, are determined by the expression (16).[3] In this case, the multipole moments are also regarded as dynamic parameters. In transition nuclei, in which both the static shape and the amplitude of the zero-point vibrations play an important role, the values of β_λ obtained by means of (16) are a superposition of both types of deformation (static and dynamic).

A list of experimental values of the quadrupole deformation parameters obtained from measured values of $B(E20\rightarrow 2)$ is given in Ref. 4, and values of $B(E3\ 0\rightarrow 3)$ are given in Ref. 5.

Another method of determining quadrupole moments (only the static moments and for nuclei with spin $I\geqslant 1$) is based on their interaction with an electric-field gradient. The quadrupole moment (spectroscopic Q_s) measured by this method is related to the intrinsic Q_0 determined by the expression (12) by a projection factor:

$$Q_s=\frac{I(2I-1)}{2I+1(2I+3)}Q_0. \tag{18}$$

It follows from the expression (11) that the difference of the mean-square charge radii of two nuclei that differ in the number of neutrons (N and N') is, up to terms quadratic in β_i,

$$\Delta\langle r^2\rangle^{N,N'}=\Delta\langle r^2\rangle_0^{N,N'}+\frac{5}{4\pi}\langle\overline{r^2}\rangle_0\sum_i\Delta\langle\beta_i^2\rangle, \tag{19}$$

where $\langle\overline{r^2}\rangle_0$ is the mean value of the radius for the compared nuclei. It can be seen that the difference can be represented in the form of two terms, one of which determines the difference of spherical nuclei at the same volume, while the other is the difference of the deformation corrections.

MODEL CALCULATIONS OF CHARGE RADII

The size and shape of nuclei and the distribution in them of the electric charge and nuclear matter are mainly determined by the nuclear forces, with respect to which the electromagnetic forces introduce only relatively small corrections. Therefore, the theoretical calculations of these nuclear properties are based on our ideas about the interaction between nucleons in nuclei. Since these ideas are as yet far from definitive understanding, all the calculations use models to describe the internucleon interactions.

The models can be divided into two groups—microscopic and phenomenological. The former are based on realistic nucleon–nucleon potentials, and in the calculations one uses the approximate methods for solving many-body problems, for example, the Hartree–Fock method. Calculations of the charge radii by this method gave comparatively good agreement with the experiments for, for example, the isotopes of Na (Ref. 6) and Sn (Ref. 7). However, each region of nuclei (or chain of isotopes) requires its own approach and specific choice of details of the internucleon potential.

The phenomenological models are based on the use of some mathematical expression containing several empirically determined parameters in order to describe the nuclear characteristics. One can then comparatively easily and at the same time in detail compare the results of calculations with experimental data and thus gauge the region of applicability of the model and the suitability of its parameters.

Among these models, the droplet model,[8,9] has been strongly developed in recent years. It describes many macroscopic properties of nuclei—their masses, the distribution of the electric charge in them, and the nuclear moments. In this model, the charge radii are given by

$$\langle r^2\rangle=\langle r^2\rangle_u+\langle r^2\rangle_r+\langle r^2\rangle_d. \tag{20}$$

The first term $\langle r^2\rangle_u$ includes a dependence on the size and shape of the nucleus for a uniform charge distribution:

$$\langle r^2\rangle_u=\frac{3}{5}R_Z^2\left(1+\alpha_2^2+\frac{10}{21}\alpha_2^3-\frac{27}{35}\alpha_2^4+\frac{10}{7}\alpha_2^2\alpha_4+\frac{5}{9}\alpha_4^2+\ldots\right), \tag{21}$$

where α is a deformation parameter that differs from the parameter β in (10) by the factor $5/4\pi$. The second term is determined by the redistribution of the charge as a result of the Coulomb repulsion of the protons:

$$\langle r^2\rangle_r=\frac{12}{175}C^1R_Z^2\left(1+\frac{14}{5}\alpha_2^2+\frac{28}{15}\alpha_2^3-\frac{29}{5}\alpha_2^4+\frac{116}{15}\alpha_2^2\alpha_4+\frac{70}{26}\alpha_4^2+\ldots\right), \tag{22}$$

where $C^1=0.0156ZA^{-1/3}$.

The third term reflects the influence of the diffuseness of the surface layer on the charge radius:

$$\langle r^2\rangle_d=3b^2, \tag{23}$$

where $b=0.99$ fm, and it is constant for all nuclei and does not depend on the nuclear shape. Further,

$$R_Z=r_0A^{1/3}(1+\varepsilon)-(N/A)t, \tag{24}$$

where t is the thickness of the neutron layer on the surface of the nucleus, ε is a correction to the nuclear radius determined by the parameters of the model, and $r=1.18$ fm.

Comparison of the charge radii calculated by means of the expressions (20)–(24) with the experimental values (with allowance for the known values of the deformation parameters α_2 and α_4) reveals over the complete range of nuclei a mean deviation 0.031 fm and a shift of the center of the deformation by 0.015 fm.

The largest deformations are observed for magic neutron numbers and at large deformations. Without allowance for the deformation of the nuclei, the agreement with the experimental data is significantly less good. This means that the shell effects are mainly manifested through the change in the nuclear shape, which is determined both by the static deformation and by the amplitude of the zero-point vibrations.

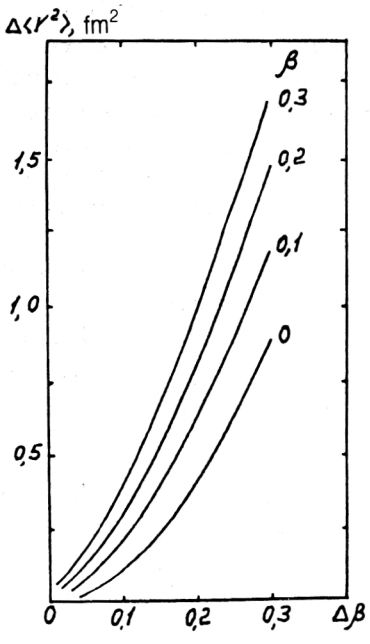

FIG. 2. Dependence of the difference of the mean-square charge radii $\Delta\langle r^2\rangle$ of nuclei with deformation parameters β and $\beta+\Delta\beta$ on $\Delta\beta$. The number next to each curve gives the initial deformation β.

It is assumed that the parameters of the model do not depend on Z, N, and the shape of the nucleus. Naturally, there is no strict justification for this, and it need not hold. For example, from several experiments it follows that the parameter b of the surface layer depends on the number of neutrons in the nucleus.[10,11]

It follows from the expressions (20)–(24) that the change in the charge radius on the addition of a pair of neutrons, $\Delta\langle r^2\rangle^{N,N+2}$, is, for unchanged deformation, ~ 0.12 fm^2 in a wide range of Z and A. The change of the deformation is here regarded as a correction to $\Delta\langle r^2\rangle$. The dependence of this correction on the change in the quadrupole deformation parameter β_2 for different initial values of this parameter is shown in Fig. 2. It can be seen that this correction $\Delta\langle r^2\rangle_\beta$ can be appreciable. For example, for a nucleus with $A=150$ and a change in β from 0.2 to 0.3 (such changes occur at the boundaries of the regions of deformed nuclei) the growth of the mean-square charge radius is 0.43 fm^2, a quantity appreciably greater than the growth when a pair of neutrons is added.

Droplet-model calculations of the changes of the charge radii are usually employed to analyze the data. The deviations of $\Delta\langle r^2\rangle$ from the values calculated for the same deformation of the compared nuclei indicate the change of the deformation. However, as will be shown below, the changes of the deformation obtained in this manner do not always correspond to independent measurements of them.

EXPERIMENTAL METHODS OF DETERMINING THE CHARGE RADII

The experimental methods of determining the charge radii (and also the parameters that describe the distribution of the electric charge in the nucleus) are based on the electromagnetic interaction of "test" particles with the nucleus. The results of the measurements will be most definite if the "test" particles have only electromagnetic interactions. Such particles are the electron and muon. These particles are used in two kinds of experiment:

1. Elastic scattering of electrons and muons by nuclei.
2. Measurement of the energies of stationary states in systems consisting of an electron or muon and a nucleus (in ordinary atoms and in mesic atoms).

Measurements of the angular distribution of electrons with energies of the order of several hundred mega-electron-volts scattered elastically by nuclei yield information about the distribution of the electric charge in the nucleus from which the parameters (c and a) of this distribution can be determined. From these parameters one can then obtain the mean-square charge radii by using the expression (8). The accuracy in the determination of $\langle r^2\rangle$ is $\sim 10^{-3}$. This is sufficient to estimate the change of the charge radii in going from one element to another but is not always sufficient for the comparison of the charge radii of isotopes of a given element. Experimental data on the parameters of the charge distribution obtained from electron elastic scattering are given in the review of Ref. 12.

The energies of quasistationary states of nucleus–muon (or nucleus–electron) systems also depend on the finite sizes of the nucleus. The energy shift is particularly large for the s states. In the case of muons, it is much higher than for electrons, since the muon masses are appreciably greater. For example, in lead the binding energy of the lowest $1s$ state of the mesic atom is ~ 10 MeV, whereas for a point nucleus it should be ~ 20 MeV. At the same time, the $2p$ states are not so dependent on the influence of the nuclear size. Therefore, measurement of the energy of the $2p\rightarrow 1s$ transition is a comparatively accurate measure of one of the parameters of the electric-charge distribution in the nucleus. Measurement of the energies of the radial transitions in the mesic atom provide a more complete picture of the charge distribution, since the different transitions are sensitive to different moments of the charge density. To the energy of each transition there corresponds a definite moment $\langle r\rangle$ of the radial charge distribution.[13] These moments can be expressed in terms of an equivalent radius,

$$R_k=[\tfrac{1}{3}(k+3)\langle r^k\rangle]^{1/k}, \tag{25}$$

where the exponent k is determined by the Z of the nucleus and is almost independent of the form of the charge distribution. For the charge radii of rare-earth elements

$$\langle r^2\rangle^{1/2}=0.782R_k^2. \tag{26}$$

The energy differences of the transitions $2p_{3/2}\rightarrow 1s_{1/2}$ and $2p_{1/2}\rightarrow 1s_{1/2}$ in the mesic atoms for neighboring isotopes are a few kilo-electron-volts and can be measured with high accuracy. This makes it possible to determine the differences of the mean-square charge radii to accuracy 5–10% and the absolute values of $\langle r^2\rangle$ to 10^{-2}%. However, because the muon beams have comparatively low intensity, such measurements can be made only with stable

isotopes available in significant amounts. The experimental values of $\Delta\langle r^2\rangle$ obtained from measurements of the spectra of mesic atoms are given in the review of Ref. 14 and in the original studies.[15–17]

In the optical and x-ray spectra, the influence of the finite nuclear size is manifested in differences of the frequencies of lines corresponding to states on which the influence of the extension of the nuclei is different. The largest energy shift occurs for the s and p states. The dependence of the energy of these states on the size of the nucleus is completely determined by the density of electrons in the neighborhood of $r=0$. In the first approximation of perturbation theory, the shift of the nth electron level relative to a point charge is given by

$$\Delta E=4\pi\int_0^\infty \rho(r)V_e(r)r^2dr, \tag{27}$$

where $V_e(r)$ is the potential due to the nth unperturbed electron, which is normalized to 0 at the origin. In the neighborhood of the nucleus, the electron density for the $s_{1/2}$ and $p_{1/2}$ states is

$$\rho_0(r_0)=-Cer^{2\sigma-2}, \tag{28}$$

where C is a normalization constant (it is larger for the $s_{1/2}$ state),

$$\sigma=\sqrt{1-(Z\alpha)^2}\cong\sqrt{1-(Z/137)^2}. \tag{29}$$

With such a description of the electron density, the expression for the level shift is

$$\Delta E=\left[\frac{4\pi Z^2eC}{2\sigma(2\sigma+1)}\right]\langle r^{2\sigma}\rangle. \tag{30}$$

For most nuclei, σ is near unity (for example, $\sigma=0.92$ for $Z=50$ and $\sigma=0.74$ for $Z=92$). Therefore, the value of $\langle r^{2\sigma}\rangle$ occurring in the expression (30) for ΔE is close to the mean-square charge radius.

In the experiments, one measures not the shifts of the energy levels relative to a point nucleus but the shifts between neighboring isotopes of a given element (the isotope shifts). For this, one measures the energies of transitions between levels that are influenced differently by the finite sizes of the nuclei. Such transitions are associated either with a change in the orbit an s electron (transitions of the type $ns\to np$ or $ns^2\to nsnp$) or with a change in the screening of the inner closed shells of s electrons (transitions of the type $nf^m\to nf^{m-1}(n+1)d$). Measurement of the energy differences of these transitions for different isotopes makes it possible to determine the change $\Delta\langle r^2\rangle$ resulting from a change in the number of neutrons in the nucleus.

The isotope shifts are measured in both the x-ray and optical range of wavelengths. In the first case, the typical values of the shifts for $2p_{3/2}\to 1s_{1/2}$ transitions are in the region of milli-electron-volts (for example, $\Delta E=30(5)$ meV for the isotopes ^{92}Mo–^{100}Mo, and $\Delta E=238(13)$ meV for the isotopes ^{144}Nd–^{150}Nd (Ref. 18)). At the same time, the line widths (for the $K_{\alpha 1}$ or $K_{\alpha 2}$ lines) reach tens of electron volts (for example, 7.2 eV for Mo and 43.0 eV for W). Such a ratio of the line width to the line shift naturally limits the accuracy and sensitivity of the measurements. At the same time, for the $1s$ and $2p$ levels there are no admixtures of other configurations, and the corrections due to the shifts resulting from other effects can be calculated quite accurately, and therefore the additional uncertainties which arise on the transition from the measured isotope shifts to the differences of the charge radii are small (as a rule, not more than 5%). A list of experimental values of $\Delta\langle r^2\rangle$ measured by the methods of x-ray spectroscopy is given in the reviews of Refs. 19 and 20.

In the case of optical spectra, the situation is different. The isotope shifts are much greater than the widths of the optical lines (respectively, 10^{-9}–10^{-8} eV and 10^{-7}–10^{-6} eV). However, the admixture of configurations in the optical levels and the uncertainty of the corrections greatly increase the error in the differences of the charge radii despite the accuracy of the measurements of the isotope shifts.

LASER METHODS FOR MEASURING ISOTOPE SHIFTS

In recent years, tunable lasers have been widely used to measure the isotope shifts and hyperfine structure of optical lines. A feature of laser experiments is that the transition energies are not measured but are specified by the wavelengths of the laser radiation at which resonances corresponding to excitation of the investigated atomic levels are observed. The width of the lasing line in lasers with frequency stabilization can be reduced to a few megahertz ($\sim 10^{-9}$ eV), and the wavelength differences of the laser radiation can be calibrated to the same accuracy (by means of a Fabri–Pero interferometer). This makes it possible to measure distances between resonances (the isotope shifts or hyperfine structure) to an accuracy that reaches 10^{-2}%. In practice, this accuracy is usually limited by the Doppler broadening of the optical line that results from the interaction of the laser radiation with atoms moving at different angles relative to the beam.

The high power of laser radiation (up to 1 W or 10^{19} photons/sec) and the large resonance cross section for absorption of a laser photon by an atom (up to 10^{-12} cm^2) have the consequence that each atom in the region of the laser radiation is excited in 10^{-7}–10^{-6} sec. If the lifetime of the atom in the excited state is of the same order, and it returns to the original state, then during the time of its passage through the laser beam (a distance of a few millimeters) it can absorb and emit up to several hundred optical photons. This makes it possible to detect each atom that enters the region of the laser beam and, thus, to achieve a high sensitivity of the measurements.

The laser methods for investigating the optical spectra of atoms can be distinguished by two criteria: 1) the method of bringing the atoms into the region of the laser radiation; 2) the method used to identify the resonance in the interaction of the laser radiation with the atoms.

As regards the first criterion, the methods are as follows:

a) Evaporation of a sample containing the investigated isotopes and formation of a parallel atomic beam by a system of collimators. Evaporation is achieved by thermal

heating of a sample in a crucible, by application of powerful laser radiation,[20] or by electron or ion beams.

b) The use of a beam of ions from a mass separator. In this case, there is excitation of either ions or atoms after neutralization of the ions in a cell with vapor of alkali elements.[21,22]

c) Evaporation of a sample in a gas cell[23] or ejection into a gas-filled region of products of nuclear reactions in a target irradiated in an accelerator.[24]

d) Accumulation of ions in an electromagnetic trap.[25]

The methods by which resonances are identified when atoms are exposed to laser radiation are as follows:

a) Resonant fluorescence of atoms in a beam, gas cell, or trap. The excited atom undergoes spontaneous decay with emission of optical radiation.

b) Multistage ionization of atoms. This uses the radiation of two or three lasers, which, as a result of successive capture of optical photons with excitation of intermediate levels, ionizes the atoms.[26]

c) Optical pumping of atoms. As a result of a whole series of successive excitation–deexcitation events, atoms are brought to one of the components of the hyperfine splitting of the ground state. Such atoms are separated either by passing them through an inhomogeneous magnetic field[27] or by measuring the anisotropy of nuclear radiation if the excited laser radiation is polarized (RADOP method).[28]

d) Light-induced drift of atoms in a buffer gas.[29] After capture of a resonant optical photon, the atoms become larger, as a result of which the diffusion coefficient decreases. Thus, one can produce a directed motion of the atoms relative to the detectors of the nuclear radiation.

Real experimental facilities, operated both in a beam of bombarding particles (in the on-line regime) and off it (off-line), are based on various combinations of these methods. The achieved sensitivity makes it possible to carry out measurements with fluxes of atoms or ions down to 10^4 sec^{-1}. In individual cases, when one is detecting particles with a very low background (for example, fission fragments), this minimum intensity of the atomic beam can be reduced still further.[30,31] Then isotopes with lifetimes down to a few milliseconds become accessible for measurement. This minimum time is mainly determined by the time required to bring the atoms to the laser beam, and in a number of cases can be greatly reduced. For example, if the investigated nucleus is formed directly in the region of the laser radiation (in a reaction or by radioactive decay), then nuclei with lifetimes down to nanoseconds can be investigated.[32] The isomer shift and hyperfine splitting of the ^{85}Rb nucleus in the isomer state, which has lifetime 1 μsec, were measured in Ref. 33. The nuclei were produced by β decay of ^{85}Kr in a gas cell.

DETERMINATION OF DIFFERENCES OF CHARGE RADII FROM ISOTOPE SHIFTS OF OPTICAL LINES

As was noted above, measurement of the difference of resonance frequencies by laser excitation of atoms (or measurement of differences of the wavelengths of optical transitions) makes it possible to determine the differences of the mean-square charge radii of the investigated isotopes. The theory of the isotope shifts of optical lines is expounded in the monograph of Ref. 34, and experimental data are given in Refs. 35–37.

The isotope shifts of optical lines of atoms with nuclei with mass numbers A and A' are determined by two factors:

$$\Delta\nu^{A,A'}=\Delta\nu_{\nu}^{A,A'}+\Delta\nu_{m}^{A,A'}, \tag{31}$$

where the first of them (the field shift) depends on the change in the volume (or charge radius) of the nucleus, while the second depends on the change in the mass:

$$\Delta\nu_{\nu}^{A,A'}=F_i\lambda^{A,A'}, \tag{32}$$

$$F_i=E_i f(Z), \tag{33}$$

where E_i and $f(E)$ are, respectively, the electron and nuclear factors (they are discussed below), and $\lambda^{A,A'}$ includes the change in the parameters of the radial distribution of the electric charge of the nucleus:

$$\lambda^{A,A'}=\Delta\langle r^2\rangle^{A,A'}+c_2/c_1\Delta\langle r^4\rangle^{A,A'}+c_3/c_1\Delta\langle r^6\rangle^{A,A'}+..., \tag{34}$$

in which c_i reflect the contribution of the moments of different orders. This contribution is practically independent of the principal quantum number of the electron shell, and therefore it is the same for optical and x-ray transitions. The values of c_i calculated for $2p\rightarrow 1s$ transitions and a Fermi distribution of the charge in the nucleus are given in Ref. 38. Using them, we can introduce a correction for the moments of higher order. If a restriction is made to the third order, then the relationship between λ and $\Delta\langle r^2\rangle$ is

$$\Delta\langle r^2\rangle^{A,A'}=\frac{1}{1+y}\left[\lambda^{A,A'}-(x-y)\Delta\langle r^2\rangle^{A,A'}\right], \tag{35}$$

where

$$x=\frac{10}{7}\frac{c_2}{c_1}\langle r^2\rangle_{\rm sph}+\frac{c_3}{c_1}\langle r^4\rangle_{\rm sph},$$

$$y=2\frac{c_2}{c_1}\langle r^2\rangle_{\rm sph}+3\frac{c_3}{c_1}\langle r^4\rangle_{\rm sph}, \tag{36}$$

in which $\langle r^2\rangle_{\rm sph}$ and $\langle r^4\rangle_{\rm sph}$ are the moments of the charge distribution calculated in the droplet model described above.[9] For this method of calculation, the difference between λ and $\Delta\langle r^2\rangle$ is 0.4% for the isotopes of Ca ($Z=20$) and 7.5% for the isotopes of Ra ($Z=88$).

Another way of taking into account the correction to the values of λ is to calculate directly the moments of these orders using the Fermi charge distribution in the nucleus and known values of the deformation parameters β_2, β_4, β_6 (Ref. 39).

The mass shift has two components—the normal mass shift (NMS) and the specific mass shift (SMS):

$$\Delta\nu^{A,A'}=\frac{A-A'}{AA'}(M_{\rm NMS}+M_{\rm SMS}), \tag{37}$$

where M_{NMS} and M_{SMS} are the constants of these shifts, with

$$M_{NMS}=5.487\cdot 10^{-4}\nu_i, \tag{38}$$

where ν_i is the frequency of the atomic transition in megahertz.

The specific mass shift arises from the influence of the correlated motion of the electrons on the recoil energy of the nucleus. Although, as can be seen from the expression (37), this shift decreases rapidly with increasing mass number of the nucleus, its contribution can be appreciable in a number of cases (tens of times higher than the normal mass shift). The values of M_{SMS} can be estimated only in the case of the pure transitions $ns\rightarrow np$,

$$M_{SMS}=(0.3+0.9)M_{NMS}, \tag{39}$$

or $ns^2\rightarrow nsnp$,

$$M_{SMS}=(0+0.5)M_{NMS}. \tag{40}$$

In the remaining cases, the values of $\Delta\nu_{SMS}$ are determined from a comparison of measured relative values of λ (after correction for the normal mass shift) and values known for the pure $ns\rightarrow np$ or $ns^2\rightarrow nsnp$ transitions or values obtained from spectra of K x rays or the spectra of mesic atoms by means of the King graph.[40]

Thus, the determination of the differences of the charge radii from measured isotope shifts reduces to allowance for the corrections for the mass shifts (normal and specific) and calculation of the electron, F_i, and nuclear, $f(Z)$, factors, which in the expression (32) relate the field shift to the change of the charge radius.

The electron factor determines the change of the total nonrelativistic density of the electron charge at the point of the nucleus, $\Delta|\psi(0)|^2$, for the measured optical transition:

$$E_i=\frac{\pi a_0^3}{Z}\Delta|\psi(0)|^2, \tag{41}$$

where Z is the atomic number of the element, and $a_0=5.29\cdot 10^{-9}$ cm is the classical Bohr radius. The values of $\Delta|\psi(0)|^2$ can be calculated sufficiently accurately only for the pure $ns\rightarrow np$ or $ns^2\rightarrow nsnp$ transitions. In the remaining cases, they are determined by comparing the measured values of $\Delta\nu$ with the values known for the pure transitions on the basis of the King graph. In this graph, the plotted quantities are the "modified" isotope shifts ε_i for the investigated line and for the pure $ns\rightarrow np$ or $ns^2\rightarrow nsnp$ transition for several pairs of isotopes:

$$\varepsilon_i=\Delta\nu_i^{A,A'}\frac{AA'}{A-A'}. \tag{42}$$

The slope of this straight line determines the ratio E_i/E_k of the electron factors, and its intercept with the X axis determines the specific mass shifts.

The nuclear factor $f(Z)$ includes corrections to the electron wave function that arise from relativistic effects and the finite size of the nucleus:

$$f(Z)=\frac{5}{2}\bar{A}^{-1/3}c^{A,A'}\left(\frac{R_{eq}}{r_0\bar{A}^{1/3}}\right)^{2\sigma-2}[r_0(A-A')]^{-1}, \tag{43}$$

where $\bar{A}=(A+A')/2$, $r_0=1.2$ fm, $R_{eq}^2=(5/3)\langle r^2\rangle$, $\sigma=1-\alpha^2Z^2$, where α is the fine-structure constant (1/137), and $c^{A,A'}$ is the theoretical constant of the isotope shift for a uniformly charged sphere with radius $R=r_0A^{1/3}$. The values of $f(Z)$ calculated by means of (43), and also their dependence on Z for nuclei in the β-stability valley are given in Ref. 41.

For nuclei with a different ratio of Z to N up to the nucleon- stability boundary, the differences of $f(Z)$ do not exceed 2%.

It can be seen from the above that the determination of the differences of the charge radii from the measured isotope shifts is a rather complicated procedure involving the introduction of several corrections which cannot always be correctly calculated. Naturally, this increases the errors in $\Delta\langle r^2\rangle$. Although the laser methods do lead to measurements of the isotope shifts with an accuracy to fractions of a percent, this accuracy is preserved only for the relative values of λ [see (32)]. The accuracy of the absolute differences of the mean-square charge radii is lowered for the pure $ns\rightarrow np$ or $ns^2\rightarrow nsnp$ transitions to 5–7%, and for mixed transitions to 10–15% or more.

Measurements of the optical spectra also yield information about other parameters of the charge distribution in nuclei—the magnetic dipole (μ) and electric quadrupole (Q_s) moments. These moments lead to hyperfine splitting of the atomic levels. The splitting has the consequence that each transition between levels with total moments F_1 and F_2 consists of a number of components, the positions of which are determined by the expressions

$$\nu(F_1)-\nu(F_2)=\nu_0+W(F_1)-W(F_2), \tag{44}$$

$$W(F_i)=\frac{A_iC_i}{2}+B_i\frac{0.75C_i(C_i+1)-I(I+1)J_i(J_i+1)}{2I(2I-1)J_i(2J_i-1)}, \tag{45}$$

where ν_0 is the frequency of the unsplit particle transition, I and J_i are the spins of the nucleus and of the level of the electron shell ($i=1$ or 2), F_i is equal to the vector sum of I and J_i, $C_i=F_i(F_i+1)-I(I+1)-J_i(J_i+1)$, and the constants A_i and B_i determine, respectively, μ and Q_s:

$$A=-\frac{\mu}{I}\frac{\langle H(0)\rangle}{J}, \tag{46}$$

$$B=-e^2Q_s\langle V_{zz}(0)\rangle, \tag{47}$$

where $H(0)$ and $V_{zz}(0)$ are the magnetic field strength and the gradient of the electric field produced by the shell of the atom at the position of the nucleus.

THE BASIC TRENDS IN THE VARIATION OF THE CHARGE RADII

Much experimental material is now available on the differences of the charge radii obtained using laser spectroscopy. Measurements have been made for more than

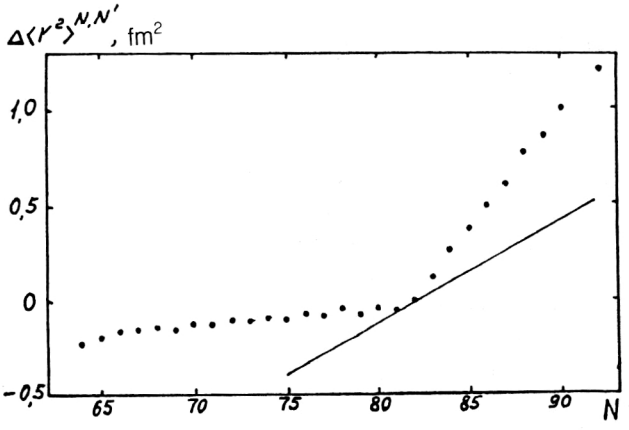

FIG. 3. Changes of the mean-square radii $\Delta\langle r^2\rangle^{N,N'}$ of the Ba isotopes relative to the nucleus with $N=82$ as functions of the number N of neutrons in the nucleus. The straight line gives the calculation in the droplet model.

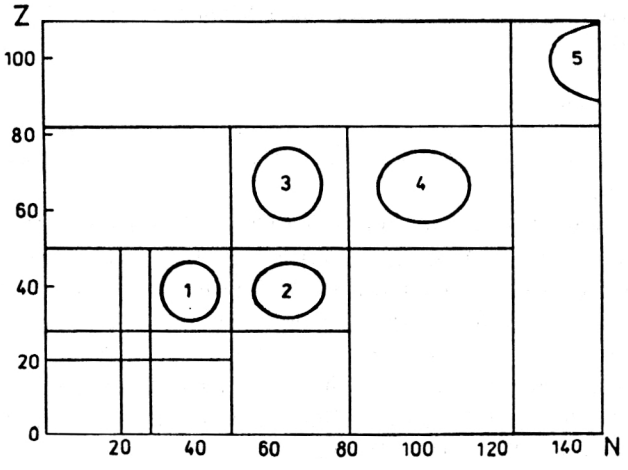

FIG. 4. Chart of isotopes. The numbers of neutrons, N, and protons, Z, in the nucleus are plotted along the X and Y axes. The straight lines show closed shells, and the ovals show the regions of deformed nuclei.

500 nuclei of elements from Na to Cm. For numerous elements, investigations have been made of long chains of isotopes, including more than 20 nuclei (for example, 26 for Hg, and 28 for Cs) in both ground and isomer states. Several general trends in the variations of the charge radii can be established from these data.

1. With increasing number of neutrons in the nucleus, the charge radii increase, as a rule, slower than expected from the well-known relation $R=r_0A^{1/3}$.

2. The deformation of the nuclei has a strong influence on the charge radii, which grow much more rapidly if the increase in the number of neutrons is accompanied by an increase in the deformation. If it is not, the charge radii grow much more weakly. In some cases, they even decrease, i.e., decrease of the deformation is manifested more strongly than growth in the volume of the nucleus. Figure 3 shows the dependence of the charge radii on the number of neutrons in a nucleus, Ba, for a long chain of isotopes.[42] The behavior of the charge radii is quite different in the region $N<82$, where the quadrupole deformation decreases as the closed neutron shell is approached, and in the region $N>82$, where the deformation increases.

3. At the boundaries of the regions of deformed nuclei we find the greatest changes: jumps in the charge radii.

4. On the addition of one neutron, the change in the charge radius is usually less than half its change on the addition of a pair of neutrons (even–odd alternation of the charge radii), although for some regions of nuclei there are exceptions to this rule.

These general trends are not always satisfied in certain regions of nuclei. For a more detailed analysis of the experimental data, we consider below individual regions of nuclei: 1) near closed proton and neutron shells; 2) on the boundaries of deformation regions; 3) in the center of deformation regions; 4) in isomer states.

The positions of these regions in the isotope chart can be seen in Fig. 4.

CHARGE RADII NEAR CLOSED PROTON SHELLS

Nuclei with closed shells have spherical (or nearly spherical) shape. Their deviations from sphericity are largely due to vibrations of the nuclear surface, the amplitude of which is relatively small. Therefore, one can expect a relatively weak influence of the deformation of the nucleus on its charge radius, while other effects that influence it, for example, those associated with closing of neutron shells, must be manifested more strongly.

Long isotope chains of nuclei with closed proton shells have been investigated for Z equal to 20 (Ca), 50 (Sn), and 82 (Pb), and also for the neighboring nuclei (isotopes of K, Cd, In, Hg, Tl), Examples of the changes of the charge radii with increasing number of neutrons in the nucleus (relative to $\langle r^2\rangle$ for the nucleus with minimum N) are shown in Figs. 5, 7, and 10. It can be seen that the dependences differ appreciably for each of the shells. To a certain degree, these differences are due to the different

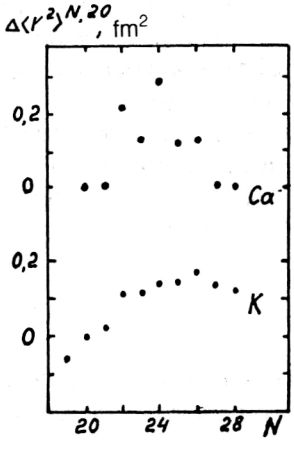

FIG. 5. Change of $\Delta\langle r^2\rangle^{N,N'}$ for the Ca and K isotopes (relative to the nucleus with $N=20$) as function of the number N of neutrons in the nucleus.

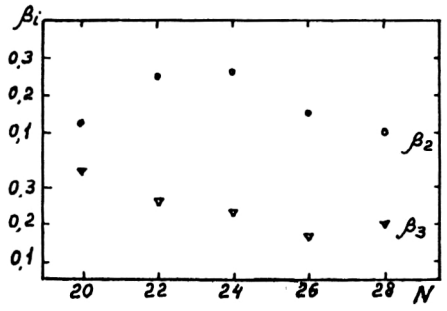

FIG. 6. Dependence of the parameters of the quadrupole, β_2, and octupole, β_3, deformation of the Ca isotopes on the number of neutrons in the nucleus.

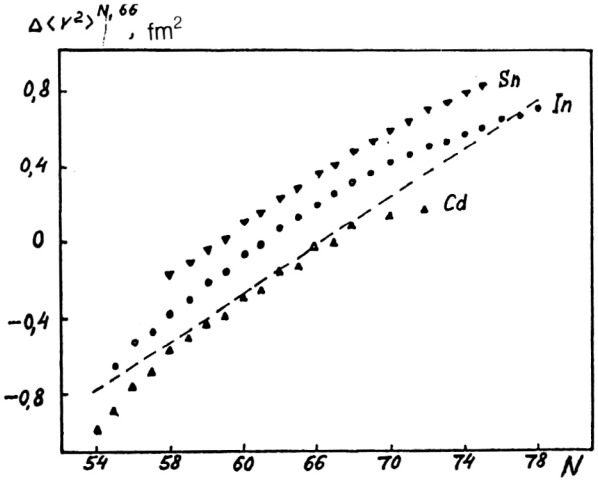

FIG. 7. Dependence of the change of the charge radii of the Cd, In, and Sn isotopes (relative to the nucleus with $N'=66$) on the number N of neutrons in the nucleus. The straight line is the calculation in the droplet model.

positions of the chains relative to the closed neutron shells. In the case of the Ca and K isotopes, the isotope chain covers the entire region between the closed shells with 20 and 28 neutrons. The chains of Cd, In, and Sn isotopes are situated in the center of the region between the shells with $N=50$ and 82, while the Hg, Tl, Pb isotopes are near a shell of 126 neutrons. All this requires a separate analysis of the behavior of the charge radii for each of the chains with a different number of neutrons in the nucleus.

In the case of the Ca isotopes, the dependence of the charge radii on the neutron number (Fig. 5) has an unusual form (compared with the other chains)—a growth in the region $N=20$–24 and a decrease on the approach to $N=28$ (Ref. 43). The isotopes ^{40}Ca and ^{48}Ca have practically the same charge radii, despite the appreciable difference in the number of neutrons. It follows from the droplet model that for the same deformation of the nuclei ^{40}Ca and ^{48}Ca the difference of their charge radii must be 0.4 fm^2. It can be assumed that the observed behavior of the charge radii of the Ca nuclei is due to the change of their deformation.

The dependence of the quadrupole, β_2 (Ref. 4), and octupole, β_3 (Ref. 5), deformation parameters on the number of neutrons in the nucleus for the Ca isotopes is shown in Fig. 6. It can be seen that the quadrupole deformation is a maximum for nuclei in the center of the region (^{42}Ca, ^{44}Ca), while the octupole deformation decreases from ^{40}Ca to ^{48}Ca. This behavior of the deformation parameters β_2 and β_3 explains qualitatively the observed N dependence of $\langle r^2\rangle$—at the beginning of the region, the rapid growth of the charge radii is due to the increase in both the number of neutrons and the quadrupole deformation, while at the end the decrease of the charge radii can be explained by the fact that the decrease of the deformation (both quadrupole and octupole) compensates the growth in the volume of the nucleus. However, calculations of the charge radii in the droplet model using the parameters adopted in it and the values of β_2 and β_3 given in Fig. 6 do not lead to quantitative agreement with the experimental data—the growth of the charge radii from ^{40}Ca to ^{48}Ca resulting from the increase in the number of neutrons (and, therefore, volume of the nucleus) is not compensated by the decrease due to the decrease in the deformation. There are evidently other factors that have a strong influence on the variation of the charge radii. They probably include the thickness of the surface layer, which can be more strongly enriched with protons of the ^{40}Ca nucleus.

The unusual behavior of the Ca nuclei concerns only their charge radii. The radii of the nucleon distributions of ^{40}Ca and ^{48}Ca determined from the elastic scattering of heavy charged particles are completely different. For example, from proton elastic scattering it follows that the difference of the mean-square nucleon radii of ^{48}Ca and ^{40}Ca is 0.16 fm^2 (Ref. 44).

In the case of the chain of K isotopes ($Z=19$),[45] the dependence of the charge radii on the number of neutrons in the nucleus is close to the one observed for Ca. However, the decrease of the charge radii on approach to the closed shell with $N=28$ is not so abrupt, and the value of $\langle r^2\rangle$ for ^{47}K ($N=28$) is 0.124 fm^2 greater than for ^{39}K ($N=20$). For the K nuclei, the deformation parameters β_2 and β_3 are not known so accurately as for the Ca nuclei. However, if their values and N dependence are the same as for Ca, then the use of them in droplet-model calculations leads to satisfactory agreement with experiment.

The changes of the charge radii between the closed shells with 50 and 82 neutrons in the isotopes of Cd (Ref. 46), In (Ref. 47), and Sn (Ref. 48) ($Z=48$–50) are shown in Fig. 7. In this case, all the N dependences of $\langle r^2\rangle$ have a similar form—a linear growth in the center of the chain, more rapid growth at the beginning, and slower growth at the end. These dependences, which resemble a parabola, can be approximated by a polynomial of second degree:

$$\Delta\langle r^2\rangle^{\bar{N},N}=a(\bar{N}-N)+b(\bar{N}-N)^2, \tag{48}$$

where $\bar{N}=66$ is the number of neutrons in the nucleus at the center of the investigated region, and a and b are parameters of the polynomial (their values are given in Table I).

TABLE I. Parameters of the parabola that describes the dependence of the charge-radius difference on the number of neutrons in the nucleus.

Z	$A-A'$	$N-N'$	a, fm^2	b, fm^2
$_{48}$Cd	102–120	54–72	0,047(1)	$-2{,}64(12)\cdot10^{-3}$
$_{49}$In	104–127	55–78	0,060(1)	$-1{,}47(13)\cdot10^{-3}$
$_{50}$Sn	108–125	58–75	0,048(1)	$-3{,}4(2)\cdot10^{-3}$
$_{70}$Yb	152–176	82–106	0,059(1)	$-2{,}4(2)\cdot10^{-3}$

Note. The number in brackets gives the error in the values.

The first of the parameters reflects the change in the volume of the nucleus. As can be seen from Table I, it is close to the change of the charge radius calculated in the droplet model for unchanged deformation. The second term takes into account the change in the deformation of the nucleus; it corresponds to $(5/4\pi)\langle r^2\rangle\Sigma_i\Delta\langle\beta_i^2\rangle$ in the expression (19). It is assumed that for $N=66$ the nucleus has maximum deformation, which decreases on the approach to $N=50$ and $N=82$.

Figure 8 shows the dependence of the parameters of the quadrupole, β_2, and octupole, β_3, deformation on the number of neutrons in the nucleus. For the isotopes of Cd and Sn, the values of β_2 and β_3 were obtained from the reduced transition probabilities, using the expression (16). Therefore, they reflect dynamic changes in the shape of the nucleus. In the case of the In isotopes, the values of β_2 are determined from the spectroscopic quadrupole moments, and they are related to the static deformation of the nucleus. It can be seen from Fig. 8 that the behavior of the quadrupole deformation does not correspond to the assumption (maximum in the center of the region). In the Cd isotopes, the values of β_2 increase with increasing N and reach a maximum at $N=72$, while in the Sn isotopes there is a decrease of β_2 in the complete investigated range of N. In addition, the changes of the quadrupole deformation parameters in the complete range of mass numbers are small (for example, β_2 varies from 0.173 for ^{106}Cd to 0.193 for ^{118}Cd or from 0.123 for ^{112}Sn to 0.095 for ^{124}Sn) and cannot be explained by the observed slope of the N dependence of the charge radii. In the In isotopes, the static quadrupole deformation parameters are close in value and also cannot explain the observed N dependence of $\langle r^2\rangle$.

As can be seen from Fig. 8, the investigated nuclei have not only a quadrupole but also an appreciable octupole deformation. In the Sn isotopes, β_3 is larger than β_2 and has a maximum in the center of the region (for ^{116}Sn). Allowance for the octupole deformation (along with the quadrupole deformation) significantly improves the agreement between the experimental values of the changes of the charge radii and those calculated in the droplet model in the case of the Sn isotopes. A similar influence of the octupole deformation on the charge radii was noted for the nuclei of Zr, which have a closed proton subshell ($Z=40$).[49] However, in the isotopes of Cd the changes in β_3 are small, and allowance for them does not eliminate the discrepancy between the calculated and experimental data. As in the Ca isotopes, there are evidently other effects that have a strong influence on the charge radii of these nuclei.

To get a more detailed picture of the changes of the charge radii, Fig. 9 shows the variation of the charge radii on the addition of a pair of neutrons, $\Delta\langle r^2\rangle^{N,N-2}$, as a function of the number of neutrons in the nucleus. It can be seen that for all chains at the beginning of the region the values of $\Delta\langle r^2\rangle^{N,N-2}$ are appreciably larger than at the end, and they are separated by the region in which the changes of the charge radii correspond to the predictions of the droplet model. It may be supposed that this behavior of the differences is due to the transition from closing of the

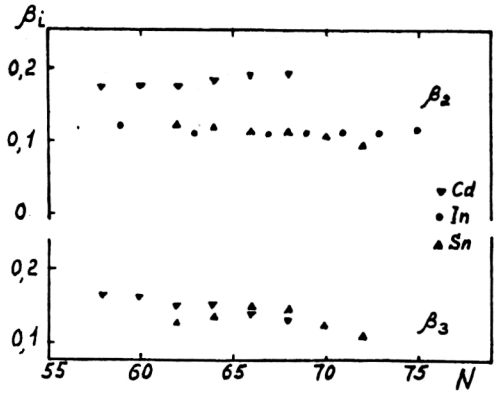

FIG. 8. Dependence of the parameters of the quadrupole, β_2, and octupole, β_3, deformation of Cd, In, and Sn on the number of neutrons in the nucleus.

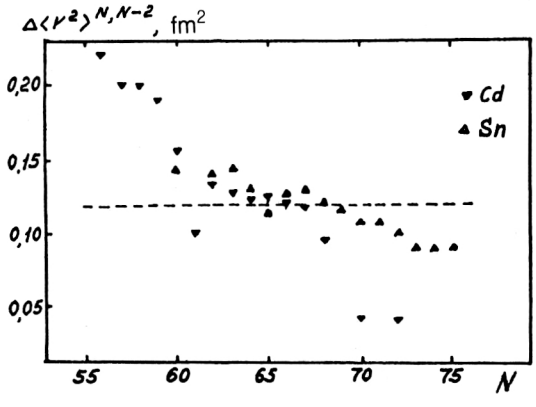

FIG. 9. Dependence of the change of the charge radii of the Cd. In, and Sn isotopes on the addition of a pair of neutrons, $\Delta\langle r^2\rangle^{N,N-2}$, on the number of neutrons in the nucleus.

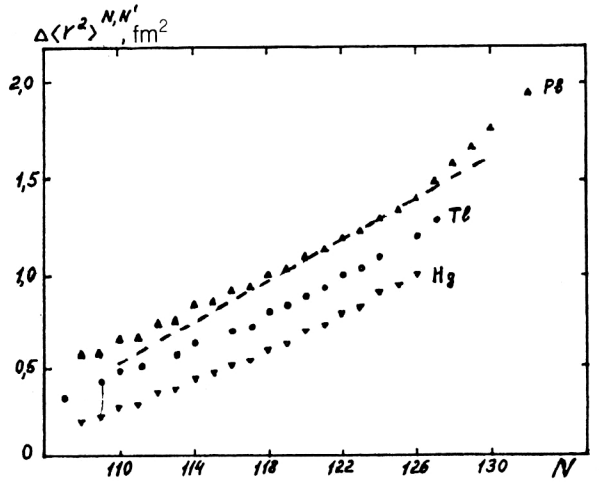

FIG. 10. Changes in the charge radii of the Hg, Tl, and Pb isotopes (relative to $N'=82$) as functions of the number of neutrons in the nucleus.

$d_{5/2}$ and $g_{7/2}$ neutron shells to the $s_{1/2}$, $d_{3/2}$, and $h_{11/2}$ shells in the region of $N=64$.

The changes of the charge radii with increasing number of neutrons in nuclei near the closed shell of 82 protons [isotopes of Hg (Ref. 50), Tl (Ref. 51), and Pb (Ref. 52)] are shown in Fig. 10. For $N<126$, there is a practically linear dependence of $\langle r^2\rangle$ on N for all elements, its slope being slightly less than that calculated in the droplet model. The inclusion of corrections for the change of the quadrupole deformation (the values of β_2 are given in Fig. 11) also practically eliminates the discrepancy.

Comparison of Figs. 5, 7, and 10 shows that with increasing atomic number the dependence on the neutron number of the charge radius of a nucleus with a closed proton shell undergoes significant changes—from a curve with a maximum for Ca to a straight line for Pb. This

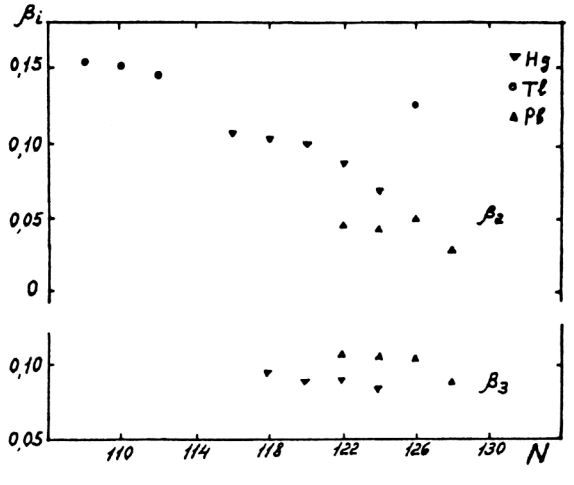

FIG. 11. Parameters of the quadrupole, β_2, and octupole, β_3, deformation of the Hg and Pb isotopes as functions of the number of neutrons in the nucleus.

difference is obviously due to the change in the contributions of the various effects to the distribution of the electric charge in the nucleus. In light nuclei, an important role is played by the surface layer and the shape of the nucleus (the deformations of various orders), and their variations with increasing N can be significant and strongly influence the changes in the charge radii. In the heavy nuclei, their importance is reduced, and the change in the volume of the nucleus with increasing number of neutrons in it becomes the main factor.

CHARGE RADII OF NUCLEI NEAR CLOSED NEUTRON SHELLS

It can be seen from Figs. 4 and 10 (chains of Ba and Pb isotopes) that the slope of the N dependence of the charge radii changes when a closed neutron shell is crossed. This can signify that the neutrons that begin to close a shell and complete its closure have different influences on the charge distribution in the nucleus and, therefore, on the charge radius. A large volume of experimental data on the changes of the charge radii of nuclei with nearly magic neutron numbers ($N=20$, 28, 50, 82, and 126) has now been accumulated. Table II gives the differences of the charge radii of nuclei with a closed neutron shell and with a number of neutrons greater than or less than 1 and 2 (data from the reviews of Refs. 35–37 were used). Table II reveals large differences in the values of $\Delta\langle r^2\rangle^{N,N'}$ for $N'<N$ and $N'>N$, but at the same time nearly equal values of these differences for nuclei of different elements differing by the same number of neutrons from the magic value. In the majority of cases, the difference of the values does not exceed the mutual errors of the measurements. The only exception is Eu ($Z-63$)—whereas for all the neighboring nuclei a slight decrease of the charge radius is observed for $N<82$, for the Eu nuclei a small growth is observed.

Figure 12 shows the dependence of the above differences of the charge radii on the number of neutrons in the nucleus near closed shells. Because of the small difference of $\Delta\langle r^2\rangle^{N,N'}$ for the different elements, we give their values averaged over Z with an error corresponding to their mean spread. It can be seen that for $N'<N$ the values of $\Delta\langle r^2\rangle^{N,N'}$ are much less than those calculated in the droplet model for spherical nuclei (0.055 fm^2 for $N'-N=1$), while for $N'>N$ they are appreciably greater. The differences are particularly large for $N=50$ and 82. Obviously, the reason for this behavior of the charge radii is the influence on them of the effects of the nuclear structure, in the first place, the deformation.

It is well known that the quadrupole deformation is least for nuclei with a closed neutron shell and increases with any change in N. One can introduce corrections for the change in the deformation, using the expressions (16) and (19), but they are too small to achieve agreement with the experimental values of $\Delta\langle r^2\rangle$. The increase in the parameter β_2 on the transition to nuclei differing by two neutrons from the magic numbers does not exceed 0.03, and this corresponds to a difference $\Delta\langle r^2\rangle_\beta^{N,N\pm2}$ of the charge radii of not more than 0.06 fm^2. However, in nuclei with

TABLE II. Differences $\Delta\langle r^2\rangle^{N,N'}$ (fm^2) of charge radii of nuclei near closed neutron shells.

N	Z	Nucleus	$N-2$	$N-1$	$N+1$	$N+2$
20	18	Ar	0,07(1)			0,17(2)
	19	K		−0,056(44)	0,021(19)	0,112(37)
	20	Ca			0,0032(25)	0,2153(49)
28	19	K	0,046(40)	0,015(20)		
	20	Ca	0,145(18)	0,009(10)		0,295(48)
	24	Cr	0,073(22)		0,062(18)	0,159(40)
50	36	Kr	0,033(7)			0,304(13)
	37	Rb	0,033(60)	0,025(34)	0,127(41)	0,283(57)
	38	Sr	0,050(2)	0,007(2)	0,124(5)	0,277(22)
	40	Zr			0,137(16)	0,224(26)
	42	Mo				0,226(19)
82	54	Xe	−0,057(7)			
	55	Cs	−0,057(15)		0,117(20)	0,270(50)
	56	Ba	−0,034(4)	−0,066(5)	0,119(8)	0,269(15)
	57	La	−0,055(27)	−0,080(10)		
	58	Ce	−0,020(4)			0,265(12)
	60	Nd	−0,021(25)	−0,062(13)	0,125(14)	0,269(26)
	62	Sm	−0,006(9)	−0,043(11)	0,123(7)	0,261(20)
	63	Eu	0,012(2)	0,040(3)	0,114(7)	0,250(14)
	64	Gd				0,30(3)
	65	Tb			0,084(9)	0,207(11)
	66	Dy	−0,013(2)			0,243(22)
	70	Yb				0,350(30)
126	80	Hg	−0,107(5)	−0,071(5)		
	81	Tl	−0,103(10)		0,099(15)	
	82	Pb	−0,109(3)	−0,068(3)	0,087(2)	0,195(3)
	87	Fr	−0,099(3)	−0,064(3)		
	88	Ra	−0,091(15)	−0,061(8)		

numbers of nucleons close to magic values an important role can also be played by more complicated changes in the shape of the nucleus, for example, the octupole deformation, as was shown above for the example of the Sn isotopes. Another factor that influences the charge radii of nuclei is their surface layer. It follows from experiments on elastic scattering of electrons by nuclei[10] that the thickness of this layer is a minimum for nuclei with closed proton and neutron shells and increases on the addition of nucleons (Fig. 13). It is possible that allowance for all these effects would lead to agreement with the observed values of $\langle r^2\rangle^{N,N'}$

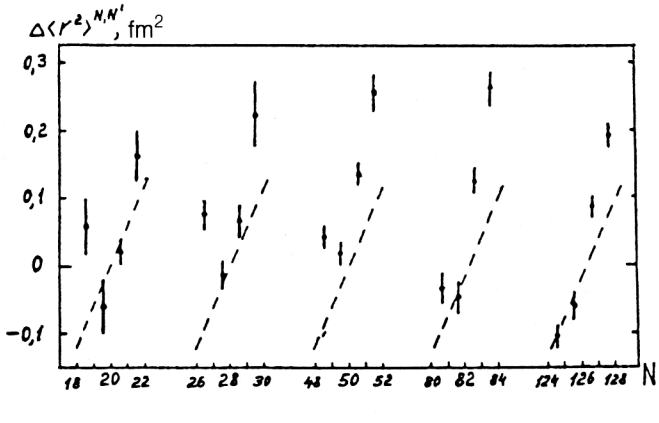

FIG. 12. Differences $\Delta(\langle r^2\rangle^{N,N'}$ of charge radii of nuclei averaged over Z (relative to the magic N') as functions of the number of added neutrons. The broken line is the calculation in the droplet model.

CHARGE RADII ON THE BOUNDARIES OF THE DEFORMATION REGIONS

As can be seen from Fig. 4, in the intervals between closed proton and neutron shells there are regions of deformed nuclei (in them, the nuclei have the shape of a prolate ellipsoid with deformation parameter $\beta_2 \sim 0.3$). Because of the strong dependence of the charge radii on the deformation parameter (Fig. 2), one must expect an appreciable growth of $\Delta\langle r^2\rangle^{N,N'}$ at the beginning of these regions, where there is also an increase in the deformation and the volume (in the neighborhoods of $N=60$, 90, and 134). Although the nuclei in these regions have been quite fully investigated (level schemes have been constructed and the values of the nuclear moments determined), measurements of the differences of the charge radii make it possible to obtain new and very important information.

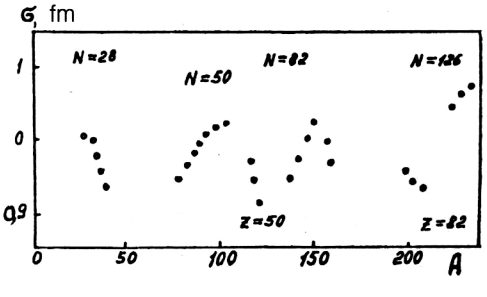

FIG. 13. Thickness σ of the surface layer of the nucleus as a function of the mass number A.

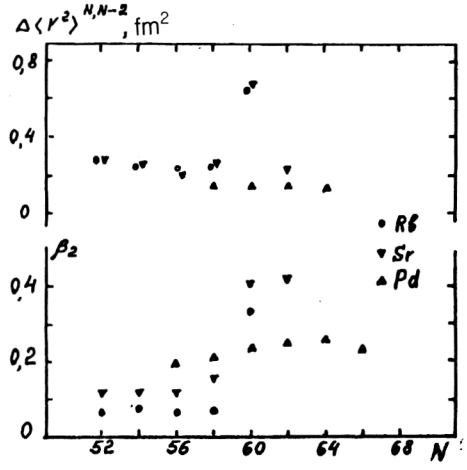

FIG. 14. Differences of charge radii of Rb, Sr, and Pd nuclei on the addition of a pair of neutrons, $\Delta\langle r^2\rangle^{N,N-2}$, and the quadrupole deformation parameters β_2 of the nuclei as functions of the number of neutrons in the nucleus.

This information makes it possible to localize reliably the place at which the transition from spherical to ellipsoidal nuclei takes place and to establish the differences between these transitions for different groups of nuclei.

Figure 14 shows the differences of the charge radii on the addition of a pair of neutrons and the quadrupole deformation parameters in the range $N=52$–64 for chains of isotopes of Rb (Ref. 53), Sr (Ref. 54), and Pd (Ref. 37) (the changes of the charge radii on the addition of one neutron are considered below). For the Sr and Pd isotopes, the parameters β_2 were obtained from the reduced probabilities of the electric quadrupole transitions[4] and include both static and dynamic deformations, while for the Rb isotopes they were obtained from spectroscopic quadrupole moments[53] and are associated only with static deformation. It can be seen that there is a jump of the $\Delta\langle r^2\rangle^{N,N-2}$ values at $N=60$ in the Rb and Sr isotopes and a smooth change in the Pd isotopes. The jump is correlated with the changes of the quadrupole deformation for all the isotopes (abrupt change of β_2 in the Rb and Sr nuclei and smooth change in the Pd nuclei). This behavior of $\Delta\langle r^2\rangle$ indicates that the transition from spherical to deformed nuclei occurs when $N=60$ is reached and in a fairly narrow range of Z (apparently, 36–42).

The known values of β_2 make it possible to estimate the contribution due to the change of the quadrupole deformation to the observed $\Delta\langle r^2\rangle^{N,N-2}$. Allowance for this contribution to the changes of the charge radii calculated in the droplet model leads to good agreement with the experimental data except for the region of N in which the transition to spheroidal shape of the nucleus occurs. In this case, the contribution due to the change in the deformation is too large—it exceeds the actual experimental values of $\Delta\langle r^2\rangle^{N,N-2}$. For example, for the pair of isotopes ^{96}Sr–^{98}Sr the experimental value is $\Delta\langle r^2\rangle=0.657(40)$ fm^2, while the correction due to the change in β_2 is 0.960 fm^2. The same thing happens for the isotope pair ^{95}Rb–^{97}Rb, although in this case allowance is made for only the change in the static quadrupole deformation. There are evidently other factors that compensate the growth of the charge radius of the nucleus on the abrupt increase of its quadrupole deformation. These may include deformations of higher orders and the thickness of the surface layer. However, the absence of data on these parameters means that we cannot draw definite conclusions about the reasons for the observed change of the charge radii.

Another region of transition from spherical to spheroidal nuclei near $N=90$ is situated mainly in the β-stability valley, and therefore experimental data on the change of the charge radii of these nuclei near this region are particularly numerous. This permits a detailed analysis of the changes of the charge radii and of the effects that influence them. Table III gives the changes of the charge radii on the addition of a pair of neutrons, $\Delta\langle r^2\rangle^{N,N-2}$, in the range $N=86$–92 and $Z=55$–70, and Fig. 15 shows the dependence of $\Delta\langle r^2\rangle$ on N in a wider range for a number of isotope chains (Refs. 55–58).

TABLE III. Differences $\Delta\langle r^2\rangle^{N,N'}$ of charge radii in the region of $N=90$.

NN' Nucleus	86—88	87—89	88—90	89—91	90–92
$_{55}$Cs	0,2639(5)	0,2215(7)	0,2155(7)		
$_{56}$Ba	0,253(15)	0,229(15)	0,216(15)		
$_{60}$Nd	0,277(26)		0,369(20)		
$_{62}$Sm	0,289(15)	0,352(24)	0,404(22)	0,351(24)	0,220(12)
$_{63}$Eu	0,292(3)	0,709(7)	0,552(5)	0,149(14)	0,106(7)
$_{64}$Gd	0,254(12)		0,430(20)		0,183(10)
$_{65}$Tb	0,299(3)	0,606(6)	0,418(4)	0,148(4)	0,099(9)
$_{66}$Dy	0,285(25)		0,371(32)		0,199(17)
$_{67}$Ho	0,303(3)	0,349(4)	0,459(4)	0,384(4)	0,140(4)
$_{68}$Er	0,270(27)		0,310(30)		0,260(26)
$_{69}$Tm			0,243(7)	0,244(7)	0,218(6)
$_{70}$Yb	0,222(20		0,219(20)		0,213(13)

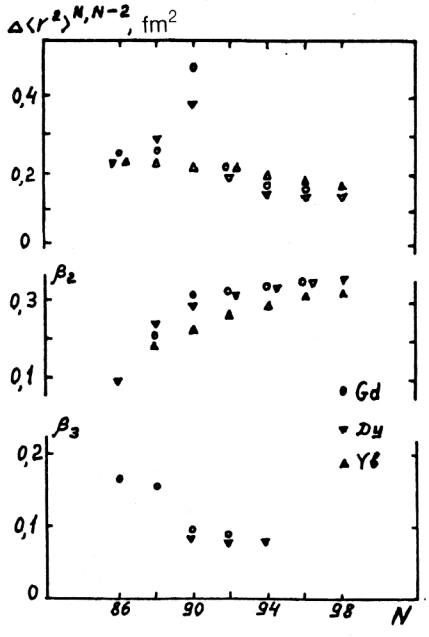

FIG. 15. Differences $\Delta\langle r^2\rangle^{N,N-2}$ of charge radii of the Gd, Dy, and Yb nuclei on the addition of a pair of neutrons and their quadrupole, β_2, and octupole, β_3, deformation parameters as functions of the number of neutrons in the nucleus.

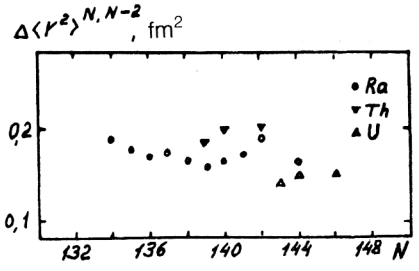

FIG. 16. Differences $\Delta\langle r^2\rangle^{N,N-2}$ of charge radii of the Ra, Th, and U nuclei on the addition of a pair of neutrons as functions of the number of neutrons in the nucleus.

It can be seen from Fig. 15 and Table III that, as at $N=60$, in the region $N=90$ there is a jump of the charge radii. However, the large set of experimental data makes it possible to identify a number of features in the behavior of the charge radii:

1. The maximum values of $\Delta\langle r^2\rangle^{N,N-2}$ (when $N=90$ is reached) are observed near $Z=64$ (isotopes of Sm, Eu, Gd).

2. With increasing distance from $Z=64$, the values of $\Delta\langle r^2\rangle^{90,88}$ decrease, and for the most distant nuclei of Cs ($Z=55$), Ba ($Z=56$), and Yb ($Z=70$) jumps of the charge radii are no longer observed.

3. For nuclei with an odd number of protons—Eu ($Z=63$) and Tb ($Z=65$)—there is a jump of $\Delta\langle r^2\rangle^{N,N-2}$ when the number of neutrons reaches 89, and not 90.

These changes of the charge radii are correlated with the change of the quadrupole deformation. The values of β_2 in Fig. 15 for nuclei with even Z were determined from the values of $B(E2\ 0\to2)$, and therefore they correspond to the sum of the dynamic and static deformations. For nuclei with odd Z, the parameters β_2 can be determined from the spectroscopic quadrupole moments and reflect only the static deformation.

Detailed analysis of the differences of the charge radii and of the static and dynamic quadrupole moments made it possible to separate the changes of these forms of deformation in the region of $N=90$ (Ref. 59). For nuclei with $N\geqslant90$ (and for the isotopes of Eu and Tb with $N\geqslant89$) the static deformation is dominant. At the same time, in nuclei with $N<90$ the two deformations are comparable in magnitude except for the odd isotopes of Sm (and, possibly, other nuclei with even Z and odd N), for which the static deformation is very small.

As for $N=60$, it is interesting to estimate the contribution to $\Delta\langle r^2\rangle^{N,N-2}$ due to the change in the quadrupole deformation of the nucleus. It was found that for nuclei with a smooth change in $\Delta\langle r^2\rangle$ allowance for this contribution to the change in the charge radius calculated in the droplet model leads to good agreement with experiment. At the same time, for nuclei in which there is a jump in $\Delta\langle r^2\rangle^{N,N-2}$ the contribution due to the change of the quadrupole deformation is too large—it exceeds the experimental values of $\Delta\langle r^2\rangle^{N,N-2}$ (Ref. 60). For example, for the isotope pair ^{150}Sm–^{152}Sm the experimental value of $\Delta\langle r^2\rangle$ is 0.404(22) fm^2, while the correction $\Delta\langle r^2\rangle_\beta$ for the change in the deformation is 0.563 fm^2. There is a similar relationship between $\Delta\langle r^2\rangle_\beta$ and $\Delta\langle r^2\rangle_{\text{exp}}$ for the isotopes of Nd, Eu, Gd, Tb.

In these isotopes, not only the quadrupole but also the octupole deformation parameters are known (Fig. 15).[5] The octupole deformation decreases with increasing N, and the greatest decrease occurs on the transition from the nucleus with $N=88$ to the nucleus with $N=90$. Allowance for both quadrupole and octupole deformation reduces the correction to the charge radius to the value $\Delta\langle r^2\rangle_{\beta_2\beta_3}$ = 0.430 fm^2. This improves the agreement between the experimental and calculated values of $\Delta\langle r^2\rangle$, but does not fully eliminate the difference.

The change of the charge radii at the boundary of the region of the heaviest deformed nuclei [the isotopes of Rn (Ref. 61), Fr (Ref. 62), Ra (Ref. 63), Th (Ref. 25), and U (Ref. 64)] is shown in Fig. 16. In the complete investigated range of N there are no significant jumps of $\Delta\langle r^2\rangle^{N,N-2}$, and there is smooth variation of the charge radii. This behavior of the charge radii can be explained by the change of the deformation. Figure 17 shows the parameters of the quadrupole,[4] octupole,[5] and hexadecapole deformations as functions of the number of neutrons in the nucleus. In the range $N=130$–140 there is a smooth growth of the quadrupole deformation (the change in β_2 does not exceed 0.05 when a pair of neutrons is added) and a decrease of the octupole deformation (smooth in the range $N=130$–134 and abrupt at $N\geqslant136$), while the hexadecapole deformation is small and hardly affects the change of the charge radii. Such smooth variation and the

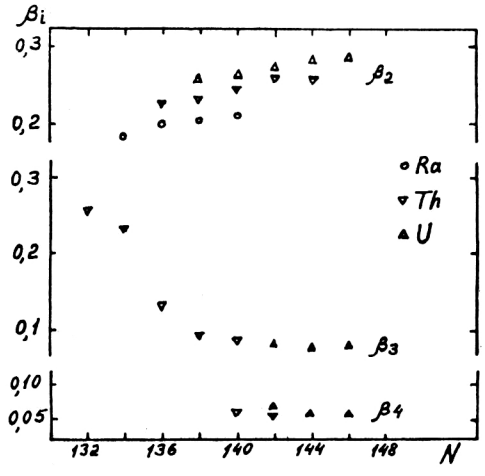

FIG. 17. Quadrupole, β_2, octupole, β_3, and hexadecapole, β_4, deformation parameters of actinide nuclei as functions of the neutron number.

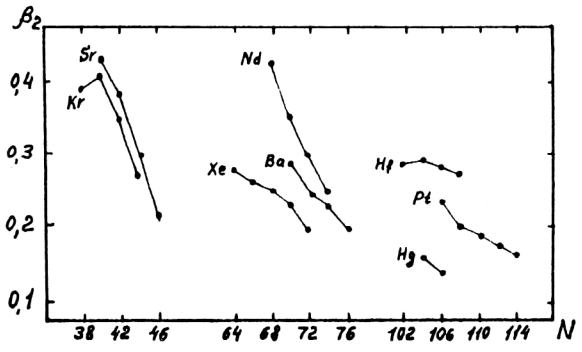

FIG. 19. Quadrupole deformation parameter of the Xe, Kr, Sr, Ba, Nd, Hf, Pt, and Hg isotopes as a function of the number of neutrons in the nucleus.

mutually compensating influence of the different forms of deformation explains the observed variations of the charge radii, which are close to the values calculated in the droplet model. The small rise in the values of $\Delta\langle r^2\rangle^{N,N-2}$ (Fig. 16) is due not to the change in the deformation but to the closing of the subshell of 142 neutrons.[63]

The close correlation between the charge radii and the deformation parameters makes it possible to estimate the change in the shape of a nucleus even when data on the deformation are not available. An example is provided by the Na isotopes. Measurements of the isotope shifts using the laser method[35] revealed a sudden growth of the charge radii from ^{25}Na ($N=14$) to ^{31}Na ($N=20$). It can be seen from Fig. 18 that the change in $\Delta\langle r^2\rangle$ for these nuclei is 1.3–1.5 fm^2, corresponding to a value ~ 0.5 of β_2 for ^{31}Na (under the assumption of a small deformation parameter ~ 0.1 for the ^{25}Na nucleus with half-magic neutron number 14). This behavior of the charge radii in the Na isotopes indicates the appearance of a new region of deformation near the magic number $N=20$ in nuclei far from the β-stability valley. The large quadrupole deformation of the neutron-rich nuclei in this region is also confirmed by a number of other effects—the higher two-neutron binding energy and the lower energy of the first 2^+ level in the

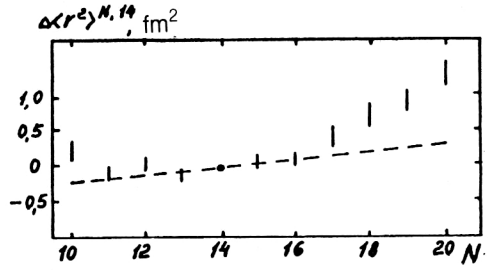

FIG. 18. Changes $\Delta\langle r^2\rangle^{N,N'}$ of the charge radii of Na isotopes (relative to the ^{25}Na nucleus with $N=14$) as functions of the neutron number.

^{32}Mg nucleus ($N=20$). Hartree–Fock calculations of the charge radii also indicate the possible appearance of a large static deformation in this region of nuclei.[6]

The regions in which there is an opposite transition from deformed to spherical nuclei are not so clearly revealed in the changes of the charge radii. In these cases, the effects that influence the charge radii work in opposite directions—the growth in the volume of the nucleus due to the increase in the number of neutrons is compensated by the decrease in the deformation. Therefore, in transition nuclei one observes either a weak growth of the charge radius or even a decrease of it.

Measurements of the differences of the charge radii on the boundaries of regions 1, 3, and 4 (Fig. 4), where a change in the shape of the nucleus occurs, were made for the isotopes of Rb (Ref. 53) and Sr (Ref. 54) (in the range $N=39$–46), Xe (Ref. 65), Cs (Ref. 66), Bs (Ref. 67), and Nd (Ref. 68) ($N=62$–74), Pt (Ref. 69), Au (Ref. 70), and Hg (Ref. 50) ($N=101$–112). Figures 19 and 20 show the dependences of these differences $\Delta\langle r^2\rangle^{N,N'}$ relative to the nuclei in which the spherical shape is established and also the quadrupole deformation parameters β_2 (Ref. 4) on the number of neutrons in the nucleus.

It can be seen from Fig. 19 that the decrease of β_2 with increasing N is strongest in light nuclei (for example, $d\beta/dN\sim 0.037$ for the Sr isotopes) and decreases with increasing Z (for Pt and Hg, $d\beta/dN\sim 0.012$). This behavior of the quadrupole deformation leads to different shapes of the N dependence of the charge radii (Fig. 20). To estimate the contributions from the quadrupole deformation, Fig. 20 shows the N dependences of $\Delta\langle r^2\rangle^{N,N'}$ for constant values of β_2 calculated in the droplet model.

As is shown in Fig. 20, the charge radii decrease with increasing N in the Rb and Sr isotopes for $N>40$. Obviously, in these nuclei the decrease of the quadrupole deformation leads to a stronger change of the charge radii than does their growth with increasing number of neutrons. In the Rb isotopes with $N<40$, the nature of the change of the charge radii is different—their decrease corresponds to small changes of the deformation. This may mean that the shape of the nucleus is stabilized at $\beta_2\sim 0.4$.

In the next transition region (Fig. 20), the nature of

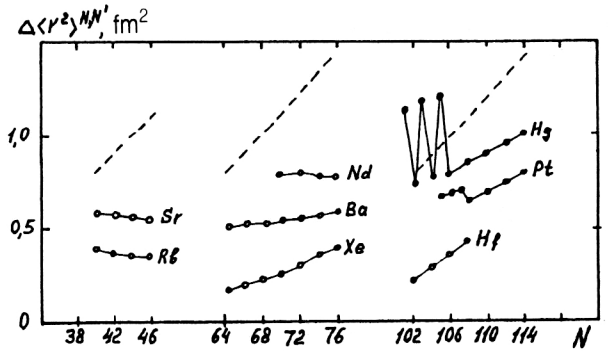

FIG. 20. Changes $\Delta\langle r^2\rangle^{N,N'}$ of the charge radii of nuclei on the deformation boundary as functions of the neutron number. The straight lines are the calculation in the droplet model.

the change of the charge radii depends on the atomic number Z of the chain of isotopes. In the Xe isotopes, there is a fairly rapid decrease of $\Delta\langle r^2\rangle^{N,N'}$ with increasing N; in the Cs and Ba isotopes, the decrease is slower, and in the Nd isotopes the charge radii hardly change. These differences in the dependences are determined by the positions of each of the chains relative to the deformation region. The chains of Xe, Cs, and Ba isotopes lie on the boundary of the region (on the side of small Z), while the chain of Nd isotopes is at its center (in the ^{128}Nd nucleus, the energy 134 keV of the first 2^+ level is lowest and the quadrupole deformation parameter is largest: 0.454 (Ref. 71)).

The most abrupt changes of the charge radii are observed at the boundary of region 4 (Fig. 4). Whereas in the Hf, W, and Os isotopes in the range $N=102$–112 there is a smooth growth of $\langle r^2\rangle^{N,N}$, corresponding to a small and smooth variation of the quadrupole deformation, in the Hg and Au isotopes with $N<108$ there are abrupt jumps of the charge radii (in the Pt isotopes, these jumps are less pronounced). At the same time, in the Hg isotopes the jumps occur only in nuclei with odd $N=101$, 103, 105, and the even–even nuclei are characterized by a smooth dependence of $\langle r^2\rangle$ on N (like all isotope chains with $N>108$).

This unusual behavior of the charge radii in the Pt, Au, and Hg isotopes is explained by the abrupt change in the shape of the nucleus with decreasing number of neutrons, namely, at $N=107$–108 there is a transition from weakly deformed oblate nuclei ($\beta_2\sim0.10$–0.15) or nuclei having the shape of a triaxial ellipsoid, to strongly deformed prolate ($\beta_2\sim0.25$) ellipsoids. In the Hg isotopes, this transition occurs only in the presence of interaction of an odd neutron with the core (or at angular momenta greater than 4).

Calculations of the differences of the charge radii in the droplet model using the experimental values of β_2 correctly reproduce the behavior of the charge radii in the Pt and Hg isotopes. The small discrepancies between the experimental and calculated values of $\Delta\langle r^2\rangle^{N,N'}$ for some pairs of isotopes can be attributed to transformations between the nuclear shape more complicated than a simple change of the quadrupole deformation or to filling of neutron shells.

CHARGE RADII OF NUCLEI IN THE CENTER OF THE DEFORMATION REGIONS

It can be expected that nuclei for which a fairly large static quadrupole deformation has already been established will be characterized by the same variations of the charge radii as for nuclei with closed proton shells. There is a large amount of experimental data on the differences of the charge radii for the deformation region with $N=90$–110. These data include long isotope chains for almost all rare-earth elements and Hf. The values of $\Delta\langle r^2\rangle^{N,N-2}$ for these nuclei are given in Table IV, from which it can be seen that there are nearly equal values of the differences of the

TABLE IV. Differences (fm^2) of charge radii of deformed nuclei.

$N-N'$	$_{63}$Eu	$_{64}$Gd	$_{65}$Tb	$_{66}$Dy	$_{67}$Ho	$_{68}$Er	$_{69}$Tm	$_{70}$Yb	$_{71}$Lu	$_{72}$Hf
90–92	0,106(7)	0,183(9)	0,094(9)	0,199(10)	0,140(2)		0,218(4)	0,213(10)		
91–93	0,035(7)	0,123(6)			0,091(4)		0,204(4)	0,210(10)		
92–94	0,129(7)	0,137(7)	0,110(8)	0,134(8)	0,110(2)		0,228(4)	0,198(10)		
93–95	0,140(6)				0,156(7)		0,190(5)	0,190(10)		
94–96	0,143(7)	0,142(8)		0,136(8)	0,123(6)	0,138(15)	0,154(2)	0,171(10)		
95–97				0,141(7)		0,143(3)	0,143(3)	0,173(10)		
96–98				0,126(7)	0,117(6)	0,113(12)	0,124(3)	0,137(8)		
97–99							0,120(3)	0,124(8)		
98–100						0,113(12)	0,126(3)	0,115(6)		
99–101							0,132(5)	0,114(8)		
100–102						0,115(12)	0,131(6)	0,107(6)		
102–104								0,084(4)	0,093(34)	0,060(9)
103–105									0,048(22)	
104–106								0,081(4)		0,060(9)

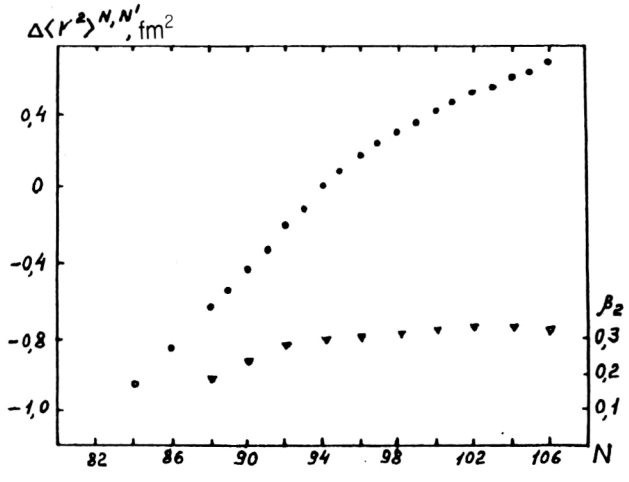

FIG. 21. Differences of the charge radii and the deformation parameter in the chain of Yb isotopes.

charge radii for nuclei with the same number of neutrons. Exceptions are the isotopes of Eu, Tb, Ho at the beginning of the deformation region (around $N=90$–94), for which the values of $\Delta\langle r^2\rangle^{N,N-2}$ are significantly lower. This difference may arise because for these isotopes the $\Delta\langle r^2\rangle$ jump (or the establishment of the deformation) occurs earlier—at $N=89$. In addition, in these nuclei there are isomer states for which $\Delta\langle r^2\rangle$ differ appreciably (the discussion of $\Delta\langle r^2\rangle$ for isomer states will be given later).

In the case of the Yb isotopes, measurements were made of the differences of the charge radii of a long chain of isotopes (for 20 nuclei from $N=82$ to $N=106$).[24,37] Their dependence on the number of neutrons in the nucleus (Fig. 21) is parabolic, as for nuclei with the number of protons close to a magic value (Cd, In, Sn. Tl, Pb isotopes). The parameters of this parabola ($a=0.060$ fm^{-2}, $b=2.4\cdot10^{-2}$ fm^{-2}) are also close to the corresponding values of those isotopes (Table I). Such a parabolic dependence corresponds to the behavior of the quadrupole deformation in the Yb nuclei, which is also shown in Fig. 21. The range of N in which the growth of β_2 occurs corresponds to the steeper rise of the charge radii; the constant values of β_2 correspond to the linear dependence, and the decay of β_2 corresponds to weak growth. This N dependence of $\Delta\langle r^2\rangle^{N,N'}$ is correctly reproduced by the droplet-model calculation using the experimental values of β_2. Although discrepancies between the experimental and calculated values of $\Delta\langle r^2\rangle^{N,N}$ are observed for individual isotope pairs, they can be attributed to the irregularities in the values of the charge radii on the filling of different neutron Nilsson orbitals (these irregularities are reproduced in calculations by the Hartree–Fock method using Skyrme forces (for example, for the Tm isotopes[72]).

EVEN–ODD DIFFERENCES OF CHARGE RADII

As a rule, the change of the charge radius on the addition of a neutron pair does not correspond to twice the change on the addition of one neutron. This irregularity in

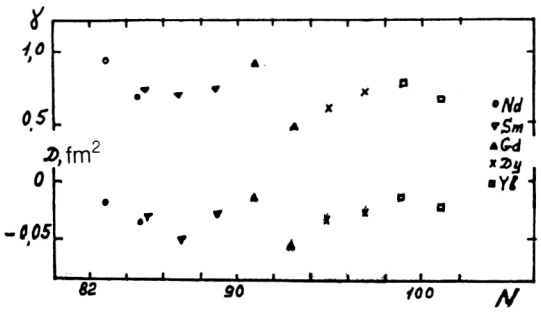

FIG. 22. Parameters of even–odd differences of rare-earth nuclei as functions of the neutron number.

the change of the charge radii is characterized by the parameters γ or D of the even–odd difference:

$$\gamma=\frac{\Delta\langle r^2\rangle^{N,N+1}}{\frac{1}{2}\Delta\langle r^2\rangle^{N+2}}, \tag{49}$$

$$D=\langle r^2\rangle^N-\tfrac{1}{2}(\langle r^2\rangle^{N-1}+\langle r^2\rangle^{N+1})$$
$$=\Delta\langle r^2\rangle^{N,N-1}-\tfrac{1}{2}\Delta\langle r^2\rangle^{N-1,N+1}. \tag{50}$$

In the majority of cases, $\gamma<1$ or $D<0$, which means that there is a weaker growth of the charge radius on the addition of an odd neutron than on the addition of an even one. The values of γ and D for various regions of nuclei are shown in Fig. 22.

This behavior can be qualitatively explained by the influence of pairing correlations on the collective potential of the nucleus. The odd neutron blocks quadrupole vibrations of the nucleus, thereby reducing its dynamic deformation $\langle\beta^2\rangle^{1/2}$ and, therefore, the charge radius. To calculate the parameters γ or D, it is also necessary to include three- and four-particle correlations.

However, there are numerous exceptions to this rule. In the neutron-deficient isotopes of Hg with $A=181$, 183, 185 mentioned above, an odd neutron polarizes the core of the nucleus, as a result of which its static quadrupole deformation increases. In the ^{152}Eu nucleus, a jump in the deformation is observed at an odd number of neutrons ($N=89$), in contrast to the remaining nuclei in this region, where the jump occurs at $N=90$.

In other regions of nuclei (Rn, Fr, Ra isotopes with neutron number $N=132$–138), anomalous values of the parameters γ or D are associated with the presence of a static octupole deformation of these nuclei. Indeed, in these nuclei we observe doublets of levels with opposite parity and enhanced reduced probabilities of $E1$ transitions between these levels. For the Th isotopes with $A=220$–230, measurements have been made of the ratios of the reduced probabilities of $E1$ and $E2$ transitions, from which the octupole deformation parameters have been determined.[73] The values of β_3 vary from 0.015 for ^{230}Th ($N=140$) to 0.25 for ^{220}Th ($N=130$). The values of β_3 are somewhat higher in the nuclei with odd N. The same situation apparently holds for the investigated isotopes of Rn, Fr, and Ra. Figure 23 shows the parameters γ and β_3 as

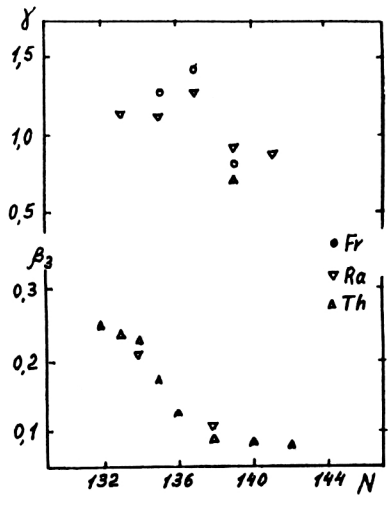

FIG. 23. Parameters of even–odd differences γ and octupole deformation β_3 of actinide nuclei as functions of the neutron number.

functions of the number of neutrons in the nucleus. It can be seen that there is a clear correlation of these parameters with $\gamma > 0$ at the maximum β_3 values.

The appearance of an appreciable octupole deformation in this region of nuclei is confirmed by the theoretical calculations of Ref. 74 on the basis of Strutinsky's shell-correction method.[75] This effect is due to the interaction between the $j_{15/2}$ and $g_{9/2}$ proton and the $j_{13/2}$ and $f_{7/2}$ neutron orbitals. In odd nuclei, the unpaired neutron changes the comparatively soft quadrupole–octupole potential, and this leads to an increase of the octupole deformation and, therefore, the charge radii.

Another region in which one observes anomalous parameters of even–odd differences not associated with the quadrupole deformation is the region of the neutron-deficient nuclei of the rare-earth elements (Eu, Tb) in the interval $N = 82$–90. It is possible that in this region a static octupole deformation is manifested.

CHARGE RADII OF ISOMER NUCLEI

Besides the measurements of the differences of charge radii of nuclei with different neutron numbers, there is much interest in analogous measurements of the change of the charge radii resulting from excitation of the nuclei (isomer shifts). Such data are usually obtained from investigations of the Mössbauer scattering of γ rays by nuclei or the x-ray spectra of mesic atoms. Although these measurements are restricted to a certain group of excited states (as a rule, those with low level energy and small change of the spins) and to only stable nuclei, a considerable amount of experimental data has by now been accumulated.[76,77]

Since isomer shifts correspond to one and the same nucleus, and its volume changes very little with increasing excitation energy, the measured differences of the charge radii in the excited and ground states, $\Delta\langle r^2\rangle_{is}$, is largely determined by the change in the shape of the nucleus. Analysis of the $\Delta\langle r^2\rangle_{is}$ values indicates that in the majority of cases the changes of the charge radii are small (they do not exceed 0.02 fm^2 or 0.01% of $\langle r^2\rangle$). This may mean that for the levels investigated by these methods the changes in the shape of the nucleus are small.

However, for some nuclei at the boundary of the deformation region, ^{153}Eu and ^{181}Ta, there are excited states with much larger, by tens of times, changes of the mean-square charge radii, and in all cases they are associated with a decrease of the charge radii. The values of $\Delta\langle r^2\rangle_{is}$ for these states, and also their properties (spin, nucleon configuration, energy) are shown in Table V. If it is assumed that the change in the shape of these nuclei is entirely due to the change of their quadrupole deformation, then from the experimental $\Delta\langle r^2\rangle_{is}$ it is possible to determine the difference of the quadrupole deformation parameters β_2 in the two states:

$$\Delta\langle\beta^2\rangle = \frac{4\pi}{5}\frac{\Delta\langle r^2\rangle_{is}}{\langle r^2\rangle}. \tag{51}$$

For these nuclei, the spectroscopic quadrupole moments Q_s are known in both the ground state and the considered excited states. Their values Q_s can be obtained by using the expression (18) and the values of the intrinsic quadrupole moments Q_0, and from them, in their turn, the quadrupole deformation parameters β_2. The values of β_2 can be compared with their difference deduced from the $\Delta\langle r^2\rangle_{is}$ values (all these quantities are given in Table V). It can be seen that the values of $\Delta\beta_2$ obtained from the different sources agree within the mutual errors. This indicates that in these nuclei there are levels characterized by smaller static quadrupole deformations.

Use of laser methods makes it possible to extend considerably the set of investigated excited states. A new region is associated with isomer states having large differences of the spins from the ground states or other selection rules preventing radiative transitions. For several isomers

TABLE V. Differences of quadrupole deformation parameters obtained from the values of the quadrupole moments and isomer shifts in experiments using Mössbauer scattering and spectra of mesic atoms.

Nucleus	E, keV	I^π	Q_s, b	β_2	$\Delta\langle r^2\rangle_{is}$, fm^2	$\Delta\beta_2$
^{153}Eu	0	$5^+/2$ [413]	2,412(21)	0,314(3)		
	97,4	$5^-/2$ [532]			−0,097(11)	−0,005(2)
	109,2	$3^+/2$ [411]	1,254(13)	0,294(3)	−0,106(12)	−0,017(2)
^{181}Ta	0	$7^+/2$ [404]	3,35(2)	0,274(2)		
	6,2	$9^-/2$ [514]	3,71(7)	0,260(6)	−0,050(15)	−0,009(3)
	482	$5^+/2$ [402]	2,35(6)	0,252(5)	−0,060(20)	−0,011(4)

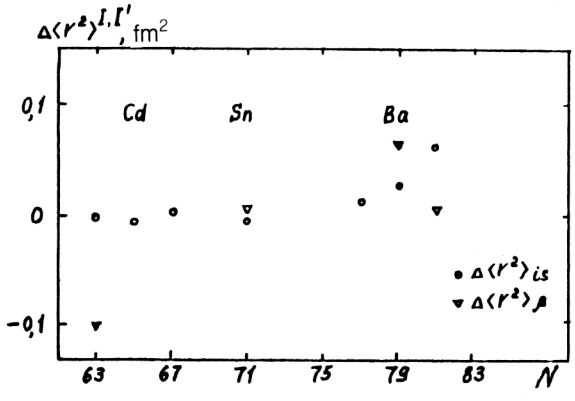

FIG. 24. Neutron-number dependence of the differences $\Delta\langle r^2\rangle_{is}$ of the charge radii in the ground and isomer $h_{11/2}$ states and of the differences $\Delta\langle r^2\rangle_\beta$ of the charge radii associated with the change of the quadrupole deformation in the nuclei Cd, Sn, and Ba.

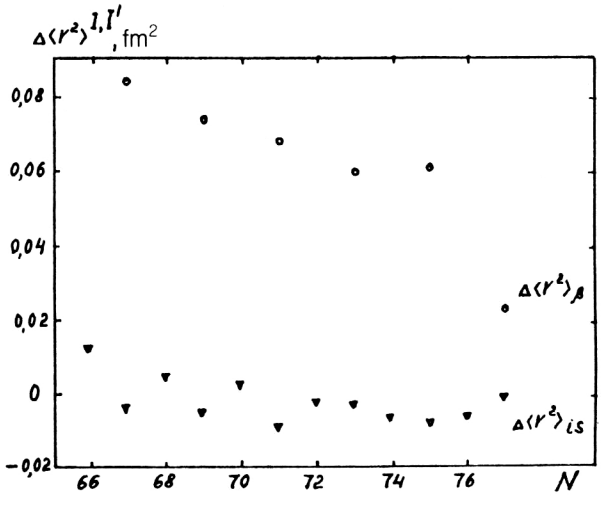

FIG. 25. The same as in Fig. 24 for isomers with $I=1/2$ and $I=8$ in In nuclei.

with the same nucleon configurations, values of $\Delta\langle r^2\rangle_{is}$ have been obtained in a wide range of Z and A, making it possible to follow the trends of their variation. Figures 24–26 show the changes of the charge radii for several isomers, namely, the differences of the charge radii between the isomer $h_{11/2}$ and ground $s_{1/2}$ or $d_{3/2}$ states in the Cd, Sn, and Ba isotopes, the differences of the charge radii between the states with $I=8$ and $I=5$ ($A=116$–122) or $I=3$ ($A=124$–126), and also with $I=9/2$ and $I=1/2$ in the In isotopes, and the differences of the charge radii between the $i_{13/2}$ and $p_{3/2}$ states in the Hg isotopes. It can be seen that in all the cases the values of $\Delta\langle r^2\rangle_{is}$ are small (<0.05 fm^2), indicating small changes in the shape of the nucleus in the isomer states. An exception is the ^{185}Hg nucleus, in which there is observed to be a significant decrease of the charge radius on the transition from the ground state to the isomer $i_{13/2}$ state. As we have already discussed, this can be explained by the coexistence of different shapes in the Hg nuclei with small (in the isomer state) and large (in the ground state) quadrupole deformation.

For some of these nuclei, the spectroscopic quadrupole moments in both the isomer and the ground states are known.[78] As a rule, they were obtained from measurements of the hyperfine structure of the optical spectra, using the laser method. As in the case of the ^{153}Eu and ^{181}Ta nuclei, the values of Q_s enable us to determine the quadrupole deformation parameters β_2 for both states. Using these values of β_2, it is possible to estimate the contribution to the difference of the charge radii due to the change of the static quadrupole deformation: $\Delta\langle r^2\rangle_{\beta_2}$. This quantity is related to the difference of the intrinsic quadrupole moment ΔQ_0 by the equation

$$\Delta\langle r^2\rangle_\beta=\frac{\Delta Q_0^2}{4Z^2\langle r^2\rangle}. \qquad (52)$$

However, it should be noted that the expression (18), which relates the spectroscopic and intrinsic quadrupole moments, is inaccurate in some cases. It holds strictly for nuclei having the shape of an axisymmetric ellipsoid.

The values of $\Delta\langle r^2\rangle_\beta$ obtained from the quadrupole moments are also shown in Figs. 24–26. Comparison of them with the values of $\Delta\langle r^2\rangle_{is}$ makes it possible to estimate the contribution to the change of the charge radii on the transition from the ground to the isomer state made by a number of effects—vibrations of the nuclear surface, deformations of higher orders, and the surface layer.

Comparison of the N dependences of $\Delta\langle r^2\rangle_{is}$ and $\Delta\langle r^2\rangle_\beta$ in Figs. 24–26 shows that, as a rule, there is no correlation between these quantities. In addition, the values of $\Delta\langle r^2\rangle_\beta$ in the majority of nuclei are significantly larger than $\Delta\langle r^2\rangle_{is}$, i.e., the change of the charge radius due to the quadrupole deformation is larger than its total change. There are two possible explanations for this difference:

1. The factors noted above, influencing the change of the charge radii (deformations of different orders, surface layer, zero-point vibrations) have a stronger effect than the quadrupole deformation.

2. The relation (18) between Q_s and Q_0, as noted above, may be inaccurate and for individual states may

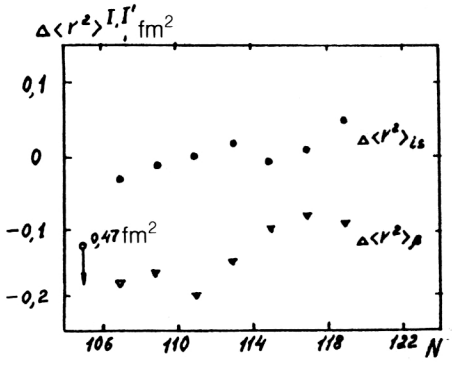

FIG. 26. The same as in Fig. 24 for $i_{13/2}$ isomers in the Hg nuclei.

TABLE VI. Differences of quadrupole deformation parameters measured by laser-spectroscopy methods.

Nucleus	N	I^{π}	Q_s, b	β_2	$\Delta\langle r^2\rangle_{is}$, fm^2	$\Delta\beta_2$
^{119}Cs	64	$9^+/2\,p[404]$	5,1(2)	0,35(1)		
		$3^+/2\,p[422]$	4,5(2)	0,31(1)	−0,198(7)	−0,036(2)
^{121}Cs	66	$3^+/2\,p[422]$	4,19(3)	0,288(2)		
		$9^+/2\,p[404]$	4,87(3)	0,335(2)	0,185(17)	0,035(4)
^{122}Cs	67	1^+		0,250		
		$8^-\,p[404]+n[532]$	3,29(8)	0,327(8)	0,184(30)	0,035(4)
^{152}Eu	89	$3^-\,p[413]+n[505]$	3,22(20)	0,35(3)		
		$0^-\,p[411]+n[532]$		0,26	−0,265(25)	−0,045(5)
^{158}Ho	91	$5^+\,p[532]+n[521]$	4,10(40)	0,317(32)		
		$2^-\,p[404]+n[521]$	1,62(17)	0,254(25)	−0,158(7)	−0,028(2)
^{185}Hg	105	$1^-/2\,n[521]$		0,26		
		$13^+/2\,i_{13/2}$	0,31(60)	0,03(6)	0,472(61)	0,15(3)

lead to underestimated values of Q_0 (or β_2). This can increase the difference ΔQ_0^2 and, therefore, $\Delta\langle r^2\rangle_{\beta}$.

Further investigations of the above effects are needed for the definitive solution of this problem.

In a number of nuclei (most of them lie on the boundary of the deformation regions), large values of $\Delta\langle r^2\rangle_{is}$ are observed. These differences of the charge radii, together with the differences of the parameters β_2 obtained from them, the quantum numbers and other characteristics of the levels, their quadrupole moments, and the values of the static quadrupole deformations are given in Table VI. It can be seen that for the majority of these nuclei there is good agreement between the values of $\Delta\beta_2$ determined from the charge radii in the isomer and ground states and the quadrupole moments of these levels.

The values of $\Delta\langle r^2\rangle_{is}$ in Table VI together with, for some levels, the quadrupole moments enable us to draw some conclusions about the properties of the transition nuclei:

1. In the region of $N=90$ in nuclei with odd Z there are isomer states with quadrupole deformation significantly lower (by 10–15%) than for the ground state, namely, in ^{152}Eu ($N=89$) (Ref. 79) and ^{158}Ho ($N=91$).[57] In ^{156}Ho ($N=89$) and ^{160}Ho ($N=93$) there are also isomer states with smaller deformation, but the difference is small ($<5\%$).

2. In the region of $N=65$ in the Cs isotopes the states with spin 9/2 are characterized by greater deformation than those with spin 3/2. In the nucleus ^{119}Cs ($N=64$) the state with larger deformation is the ground state, while in ^{121}Cs ($N=66$) it is the isomer state.

3. In the neutron-deficient isotopes of Rb in the case of the ground states the quadrupole deformation increases as $N=42$ is approached. At the same time, in the $g_{9/2}$ isomer states of the same nuclei it hardly changes ($\beta_2\sim0.16$). In the nucleus ^{85}Rb ($N=48$), which is close to a closed neutron shell, the deformation of the isomer is greater than in the ground state, while in the nucleus ^{81}Rb ($N=44$) it is less (this nucleus is strongly deformed in the ground state).

4. The Hg nuclei in the $i_{13/2}$ isomer states have small deformation. For them, no change of shape (jump of the deformation) is observed for $N<106$.

Shape isomers having enhanced quadrupole deformation[80] must, in accordance with (19), be characterized also by charge radii significantly larger than in the ground state. This will lead to anomalously large isomer shifts for such states. Indeed, the measurements in the case of the spontaneously fissioning isomer ^{242m}Am found the large isomer shift 70 GHz (Ref. 30), corresponding to a difference 5.1(2) fm^2 of the mean-square charge radii and a quadrupole deformation $\beta_2\approx0.6$ of the nucleus in the isomer state.

Thus, the laser method possesses unique possibilities for the investigation of shape isomers. The discovery of nuclear levels with anomalously large isomer shifts (several tens of gigahertz) unambiguously indicate that they have an enhanced deformation and helps to identify their nature.

CONCLUSIONS

The extensive experimental material on the charge radii of nuclei presented in this review has made it possible to follow the change of the collective and single-particle properties of the nuclei with increasing number of neutrons in a wide range of mass numbers up to the nucleon-stability boundary. Some of these properties—the deformation of the nucleus, and the amplitude of the zero-point vibrations of the nuclear surface—have a strong influence on the charge radius. Therefore, from the systematized values of the charge radii, and also using other nuclear characteristics (spectroscopic quadrupole moments, spins, magnetic moments, and reduced probabilities of electric quadrupole transitions), one can clearly identify the regions of strongly deformed nuclei or those having large amplitude of the zero-point vibrations of the surface.

Such analysis has made it possible to identify a new region of deformed nuclei—in the region $N=20$ in the Na isotopes—and also to establish that the transition to the

deformation region at $N=90$ is very different for nuclei with different Z, namely, near the half-magic value $Z=64$ there is a jump of the deformation parameters, but at some distance from it ($\Delta Z \geqslant 6$) there is a smooth transition.

Another interesting feature of nuclei at the boundaries of the deformation regions is the coexistence of different shapes in them. In the Rb, Cs, Eu, Ho, Hg isotopes isomer states with deformation appreciably greater than in the ground state have been found. The energies of these states are low (not more than hundreds of kilo-electron-volts), and in some nuclei they are the ground states (for example, in ^{121}Cs).

The differences of the charge radii are very sensitive to the predictions of the various models and can be used to test the regions of their validity. From comparison of the experimental values of $\Delta\langle r^2\rangle$ with those calculated in the droplet model one may conclude that near closed shells the model values $\Delta\langle r^2\rangle$ are lower than the experimental values, while at the boundaries of the deformation regions they are higher. To reconcile the differences, it is evidently necessary to correct the parameters of the model. At the same time, microscopic Hartree–Fock calculations that use real internucleon interactions and correctly describe numerous nuclear properties (masses, moments) lead to good agreement with experiment for the charge radii too. As has been shown in several studies,[81,82] such calculations using effective Skyrme forces correctly reproduce the changes of the charge radii in long chains of deformed nuclei.

The large group of experimental data presented in the review indicates the prospects for using laser methods in investigations of nuclear structure. These methods are still far from exhausted, and will undoubtedly provide a new source of information on nuclei.

[1] R. C. Barrett and D. F. Jackson, *Nuclear Sizes and Structure* (Clarendon Press, Oxford, 1972).
[2] A. Bohr and B. R. Mottelson, *Nuclear Structure*, Vol. 1 (Benjamin, New York, 1969) [Russ. transl., Mir, Moscow, 1971].
[3] K. Kumar, Phys. Lett. **28**, 249 (1972).
[4] S. Raman, C. H. Malarkey, W. T. Milner *et al.*, At. Data Nucl. Data Tables **36**, 1 (1987).
[5] R. H. Spear, At. Data Nucl. Data Tables **42**, 55 (1989).
[6] X. Campi, H. Flocard, A. K. Kerman, and S. Koonin, Nucl. Phys. **A251**, 193 (1975).
[7] J. Dobaczewski, H. Flocard, and J. Treiner, Nucl. Phys. **A422**, 103 (1984).
[8] W. D. Myers, *Droplet Model of the Nucleus* (IFI, Plenum, New York, 1977).
[9] W. D. Myers and K. Schmidt, Nucl. Phys. **A410**, 61 (1983).
[10] J. Friedrich and N. Voegler, Nucl. Phys. **A373**, 192 (1982).
[11] I. Angeli, J. Phys. G **17**, 439 (1991).
[12] H. de Vries, C. W. de Jager, and C. de Vries, At. Data Nucl. Data Tables **36**, 495 (1987).
[13] K. W. Ford and J. G. Willis, Phys. Rev. **185**, 1429 (1969).
[14] R. Engfer, H. Schnewly, J. L. Vuilleumier *et al.*, At. Data Nucl. Data Tables **14**, 509 (1974).
[15] J. Zumbo, B. Shera, Y. Tanaka *et al.*, Phys. Rev. Lett. **53**, 1888 (1984).
[16] E. B. Shera, M. V. Hoehn, and G. Fricke, Phys. Rev. C **39**, 195 (1989).
[17] D. Laubacher, I. Tanaka, and R. M. Steffen, Phys. Rev. C **27**, 1772 (1983).
[18] F. Boehm and P. Lee, At. Data Nucl. Data Tables **14**, 605 (1974).
[19] O. I. Sumbaev, *Intern. Symposium on Nuclear Structure* (JINR, Dubna, 1968).
[20] Yu. P. Gangrskiĭ, S. G. Zemlyanoĭ, I. N. Izosimov *et al.*, Prib. Tekh. Eksp. **1**, 168 (1990).
[21] G. Ulm, J. Eberz, G. Huber *et al.*, Z. Phys. A **321**, 395 (1985).
[22] A. C. Mueller, F. Buchinger, W. Klempt *et al.*, Nucl. Phys. **A403**, 234 (1983).
[23] P. Dabkiewicz, F. Buchinger, H. Fisher *et al.*, Phys. Lett. **82B**, 199 (1979).
[24] J. Billowes, Hyp. Interact. **59**, 3 (1990).
[25] W. Kalber, J. Rink, K. Bekk *et al.*, Z. Phys. A **334**, 103 (1989).
[26] G. D. Alkhazov, A. E. Barzakh, and É. E. Berlovich, Pis'ma Zh. Eksp. Teor. Fiz. **40**, 95 (1984) [JETP Lett. **40**, 836 (1984)].
[27] H. T. Duong and J. L. Vialle, Opt. Commun. **12**, 71 (1974).
[28] J. Bonn, G. Huber, H. Kluge *et al.*, Z. Phys. A **272**, 375 (1975).
[29] V. D. Antsygin, S. N. Atutov, F. Kh. Gel'mukhanov *et al.*, Pis'ma Zh. Eksp. Teor. Fiz. **30**, 262 (1979) [JETP Lett. **30**, 243 (1979)].
[30] C. E. Bemis, J. R. Boene, J. P. Young *et al.*, Phys. Rev. Lett. **43**, 1854 (1979).
[31] H. Backe, Th. Blonnigen, M. Dahlinger *et al.*, Hyp. Interact. (in press).
[32] D. F. Zaretskiĭ and A. V. Kozlinskiĭ, Yad. Fiz. **31**, 891 (1980) [Sov. J. Nucl. Phys. **31**, 461 (1980)].
[33] G. Shimkaveg, W. W. Quiwers, R. R. Dasari *et al.*, Phys. Rev. Lett. **53**, 2230 (1984).
[34] W. H. King, *Isotope Shifts in Atomic Spectra* (Plenum, New York, 1984).
[35] E. W. Otten, *Treatise on Heavy-Ion Science*, Vol. 8 (1989), p. 517.
[36] K. Heulig and A. Steudel, At. Data Nucl. Data Tables **14**, 613 (1974).
[37] P. Aufmuth, K. Heulig, and A. Steudel, At. Data Nucl. Data Tables **37**, 455 (1987).
[38] E. C. Seltzer, Phys. Rev. **188**, 1916 (1969).
[39] M. Wakasugi, T. Horigushi, Wei Guo Jin *et al.*, J. Phys. Soc. Jpn. **59**, 2700 (1990).
[40] W. H. King, J. Opt. Soc. Am. **53**, 638 (1963).
[41] D. Zimmermann, Z. Phys. A **321**, 23 (1985).
[42] K. Wendt, S. A. Ahmad, F. Buchinger *et al.*, Z. Phys. A **318**, 125 (1984).
[43] A. Andl, K. Bekk, S. Goring *et al.*, Phys. Rev. C **26**, 2194 (1982).
[44] G. D. Alkhazov, T. Bauer, R. Bertini *et al.*, Nucl. Phys. **A280**, 365 (1977).
[45] F. Touchard, P. Guimbal, S. Buttenbach *et al.*, Phys. Lett. **108B**, 169 (1982).
[46] F. Buchinger, P. Dabkiewicz, H. Kluge *et al.*, Nucl. Phys. **A462**, 305 (1987).
[47] J. Eberz, U. Dinger, G. Huber *et al.*, Nucl. Phys. **A464**, 9 (1987).
[48] M. Anselment, K. Bekk, A. Hanser *et al.*, Phys. Rev. C **34**, 1052 (1986).
[49] Yu. P. Gangrskiĭ, S. G. Zemlyanoĭ, B. K. Kul'dzhanov *et al.*, Zh. Eksp. Teor. Fiz. **94**, No. 6, 9 (1988) [Sov. Phys. JETP **67**, 1089 (1988)].
[50] G. Ulm, S. K. Battacherjee, P. Dabkiewicz *et al.*, Z. Phys. A **325**, 247 (1986).
[51] J. A. Bounds, C. R. Bingham, H. K. Carter *et al.*, Phys. Rev. C **36**, 2560 (1987).
[52] M. Anselment, W. Faubel, S. Goring *et al.*, Nucl. Phys. **A451**, 471 (1986).
[53] C. Thibalt, F. Touchard, S. Buttenbach *et al.*, Phys. Rev. C **23**, 2720 (1981).
[54] F. Buchinger, E. B. Ramsay, E. Arnold *et al.*, Phys. Rev. C **41**, 2883 (1990).
[55] A. N. Zherikhin, O. N. Kompanets, V. S. Letokhov *et al.*, Izv. Akad. Nauk SSSR, Ser. Fiz. **86**, 1249 (1984).
[56] S. A. Ahmad, W. Klempt, C. Ekstrom *et al.*, Z. Phys. A **321**, 35 (1985).
[57] G. D. Alkhazov, A. E. Barzakh, V. P. Denisov *et al.*, Z. Phys. A **337**, 367 (1990).
[58] G. D. Alkhazov, A. E. Barzakh, I. Yu. Chubukov *et al.*, Nucl. Phys. **504**, 549 (1989).
[59] G. D. Alkhazov, É. E. Berlovich, Kh. Vagner *et al.*, Preprint 1006 [in Russian], Leningrad Institute of Nuclear Physics (1984).
[60] S. K. Borisov, Yu. P. Gangrskiĭ, Ch. Gradechny *et al.*, Zh. Eksp. Teor. Fiz. **93**, 1545 (1987) [Sov. Phys. JETP **66**, 882 (1987)].
[61] W. Bochers, R. Neugart, E. W. Otten *et al.*, Hyp. Interact. **34**, 25 (1987).
[62] A. Coc, C. Thibault, F. Touchard *et al.*, Nucl. Phys. **A468**, 1 (1987).
[63] S. A. Ahmad, W. Klempt, R. Neugart *et al.*, Nucl. Phys. **A483**, 244 (1988).
[64] Yu. P. Gangrskiĭ, S. G. Zemlyanoĭ, B. K. Kul'dzhanov *et al.*, Izv. Akad. Nauk SSSR, Ser. Fiz. **54**, 830 (1990).

[65] W. Borchers, E. Arnold, W. Neu *et al.*, Phys. Lett. **216B**, 7 (1989).
[66] C. Thibault, F. Touchard, S. Buttenbach *et al.*, Nucl. Phys. **A367**, 1 (1981).
[67] A. C. Mueller, F. Buchinger, W. Klempt *et al.*, Nucl. Phys. **A403**, 234 (1983).
[68] G. D. Alkhazov, A. E. Barzakh, N. B. Buyanov *et al.*, Izv. Akad. Nauk SSSR, Ser. Fiz. **52**, 1651 (1988).
[69] H. T. Duong, J. Pinard, S. Liberman *et al.*, Phys. Lett. **217B**, 401 (1989).
[70] G. Savard, J. E. Crawford, J. K. P. Lee *et al.*, Nucl. Phys. **A512**, 241 (1990).
[71] R. Moscrop, M. Campbell, W. Gellelty *et al.*, Nucl. Phys. **A499**, 565 (1989).
[72] A. E. Barzakh and V. E. Starodubskiĭ, Preprint 1143 [in Russian], Leningrad Institute of Nuclear Physics (1985).
[73] P. Schuler, C. Lauterbach, E. K. Agarwal *et al.*, Phys. Lett. **174B**, 241 (1986).
[74] W. Nazarewicz, P. Olanders, I. Ragnarsson *et al.*, Nucl. Phys. **A429**, 269 (1984).
[75] V. M. Strutinsky, Nucl. Phys. **A420**, 95 (1967).
[76] G. H. Kalvius, *Hyperfine Interactions in Excited Nuclei* (IFI, Plenum, New York, 1971).
[77] H. Backe, R. Engfer *et al.*, Nucl. Phys. **A234**, 469 (1974).
[78] P. Raghavan, At. Data Nucl. Data Tables **42**, 189 (1989).
[79] G. D. Alkhazov, E. E. Berlovich, V. P. Denisov *et al.*, Z. Phys. A **316**, 123 (1984).
[80] S. M. Polikanov, *Shape Isomerism in Nuclei* [in Russian] (Atomizdat, Moscow, 1977).
[81] V. I. Kuprikov *et al.*, Yad. Fiz. **49**, 1572 (1989) [Sov. J. Nucl. Phys. **49**, 973 (1989)].
[82] V. S. Letokhov, V. I. Mishin, S. K. Sekatsky *et al.*, J. Phys. G **18**, 1177 (1992).

Translated by Julian B. Barbour